



OPEN Preparation of gold nanoparticles decorated UiO-66-NH₂ incorporated epichlorohydrin and cyclodextrin as novel efficient catalyst in cross coupling and carbonylative reactions

Leila Mohammadi & Mohammadreza Vaezi

This study presents a new, highly effective, and reusable catalyst: UiO-66-NH₂@Epichlorohydrin@Cyclodextrin@Au-NPs. This innovative catalyst starts with the Zr-based UiO-66 material, which is functionalized with amino groups (–NH₂). We enhanced its surface compatibility by modifying it with epichlorohydrin and cyclodextrin via a post-synthesis modification method. Gold nanoparticles were then stabilized on this modified composite, resulting in the UiO-66-NH₂@Epichlorohydrin@Cyclodextrin@Au-NPs complex. We used this catalyst for C–C coupling and Carbonylative Sonogashira reactions in mild conditions. Its effectiveness was underscored by various analytical techniques, including XRD, EDS, SEM, FT-IR, TEM, BET, ICP, TGA, and elemental mapping. The catalyst exhibited exceptional performance in Sonogashira, Heck, Suzuki coupling, and Carbonylative reactions, achieving good to excellent yields. It proved to be highly recyclable, maintaining its catalytic activity for up to nine cycles with minimal loss.

Gold-catalyzed C–C cross-coupling reactions, also known as Suzuki–Miyaura Coupling (SMC) reactions, are among the excellent methods for forming carbon–carbon (C–C) bonds, gaining significant attention from both industrial and academic sectors. So far, many different gold catalysts, both homogeneous and heterogeneous, have been employed to catalyze these reactions^{1–9}. While homogeneous catalysts are known for their superior catalytic performance and selectivity due to their good solubility, their industrial application is hindered by challenges in separating the catalysts from products and recovering them. In contrast, heterogeneous catalysts address these issues effectively^{10–15}. Catalysis has revolutionized human life and industrial production, playing a crucial role in numerous processes^{16–21}. Metal nanoparticles (NPs) represent an important and emerging class of heterogeneous catalysts, extensively used in a variety of reactions^{22–27}. Gold nanoparticles, in particular, are highly sensitive and exhibit significant catalytic activity due to their high surface energy. However, their small particle size makes them prone to aggregation during reactions. Immobilizing gold nanoparticles on substrates mitigates this issue by providing stability and selectivity, allowing the nanoparticles to maintain their small size and facilitating good deposition through interconnected pores^{28,29}. As a result, there has been increasing interest in developing efficient, sustainable, and recyclable gold catalytic systems, considering both economic and biocompatibility aspects. In recent years, researchers have successfully incorporated gold metal nanoparticles into metal–organic frameworks (MOFs), creating new catalytic systems by immobilizing metal complexes or nanoparticles within MOFs. This innovation aims to harness the potential of new heterogeneous catalysts in C–C cross-coupling reactions^{10,30–35}.

Metal–organic frameworks (MOFs) represent an exciting and innovative class of porous crystalline materials. They comprise metal ions and multifunctional organic ligands. MOFs are of significant interest in scientific communities for their numerous advantages, including tunable porosity, adjustable pore sizes, flexibility, high specific surface area, excellent stability, and the potential for high performance and activity. Additionally, their structural design ability makes them particularly appealing to researchers^{36–45}. Among various MOFs, the UiO

Department of Nano Technology and Advanced Materials, Materials and Energy Research Center, Karaj, Iran.
✉ email: l.mohammadi3790@gmail.com; m_r_vaezi@merc.ac.ir

(University of Oslo) series, including UiO-66^{46–48}, UiO-67^{49,50}, UiO-68^{51–54}, have garnered attention for their remarkable chemical and thermal stability. These materials exhibit tolerance to acidic conditions (pH < 1) and high temperatures (exceeding 500 °C), surpassing many other MOFs in durability^{55–59}. Moreover, metal–organic frameworks can produce a wide range of derivatives by incorporating various linkers, such as terephthalic acid (BDC), leading to functional derivatives^{55,60}, including UiO-66-NH₂^{61,62}, UiO-66-OH^{58,63}, UiO-66-COOH^{64–66}, UiO-66-NO₂^{67–70}, and others^{46,71}. However, the complexity of the organic linker can influence the coordination between the metal and ligand, potentially modifying and enhancing the MOF structure^{72,73}.

UiO-66-NH₂ is an MOF based on zirconium that includes amine groups. Its crystal structure consists of hexameric Zr₆O₃₂ units and 2-aminoterephthalate ligands^{61,74–76}. The topological structure of UiO-66-NH₂ features an octahedral cluster of Zr₆O₄(OH)₄ coordinated with twelve amino-terephthalic acid ligands. UiO-66-NH₂ is particularly suitable for post-synthesis modification (PSM) due to its structural characteristics. MOFs with NH₂ groups are known for their high adsorption capacity, which is attributed to their significant porosity and the formation of charge transfer complexes between NH₂ groups and target molecules. Consequently, surface modification of UiO-66-NH₂ through the PSM method with polymer compounds enhances the MOF's surface compatibility. Furthermore, its potential as a heterogeneous catalyst makes it valuable for various applications^{61,77}.

Cyclodextrin (CD, C₄₂H₇₀O₃₅) is a carbohydrate macromolecule derived from starch by catalytic enzymes. It is composed of a cyclic oligosaccharide featuring seven D-glucopyranose units linked together by alpha-1,4-glycosidic bonds^{78–82}. A notable feature of cyclodextrin is its unique structure: a hydrophilic outer surface and a hydrophobic central cavity. This structure allows cyclodextrin to interact with various organic and inorganic compounds via hydrogen and van der Waals bonds, leading to the formation of stable host–guest complexes^{83–86}. Cyclodextrins and their derivatives, being natural starch-derived molecules, have a high capacity for forming complexes in solution or in the solid state through host–guest interactions^{87–90}. Cyclodextrins are widely used despite their low aqueous solubility^{91–95}. They are highly effective for modifying the structure and enhancing the physical and chemical characteristics of UiO-66-NH₂. Additionally, cyclodextrins can act as inhibitors or ligands with metal cations, which improves biocompatibility, increases porosity, and provides responsiveness to stimuli through host–guest interactions^{83,96–98}.

Lately, a novel and efficient strategy has been developed to integrate cyclodextrin into UiO-66-NH₂ metal–organic frameworks (MOFs) under milder preparation conditions, without compromising the framework's ability to absorb and store guest molecules^{92,99,100}. This approach involves first enhancing the thermal stability of UiO-66-NH₂ and then incorporating biocompatible cyclodextrin into the material. The incorporation of cyclodextrin into MOFs results in the formation of new hybrid compounds due to strong molecular interactions, including metal–ligand interactions, hydrogen bonds, host–guest interactions, and covalent bonds^{101–104}. These cyclodextrin-coated or modified MOFs are synthesized to improve aqueous solubility and biocompatibility. The process of bridging cyclodextrin with MOFs presents significant challenges. Researchers in supramolecular chemistry, metal-bonded materials, and polymer chemistry have significantly advanced this field. This research highlights the strategy of combining UiO-66-NH₂ with epichlorohydrin and cyclodextrin, exploring the interactions and bonds between epichlorohydrin, cyclodextrin, and the MOF components, as well as the characteristics of the resulting materials.

Cross-linked polymers, produced through the (co)polymerization of cyclodextrin molecules and coupling agents in an alkaline environment, have attracted much attention for their straightforward synthesis, high absorption properties, and specific selectivity^{105–108}. Among the various methods, chemical cross-linking with epichlorohydrin is particularly notable for creating a water-insoluble cyclodextrin network, which is advantageous for environmental applications.

To this end, MOFs are ideal hosts. Given their permanent porosity, they offer significant advantages for confining metal nanoparticles, allowing the metal to retain its large and uniform potential, which benefits advanced catalytic applications. Recent studies have reported extensively on metallic MOF-nanoparticles (MOF@NP), highlighting their catalytic activity, which is largely attributed to the high activity and recyclability of metal nanoparticles immobilized within MOFs. The chemical environment surrounding the guest metal nanoparticles can be readily modified through functional group linkages, enhancing the catalytic performance by optimizing metal substitution within MOFs^{29,34,35,98,109–117}.

In this study, UiO-66-NH₂, known for its inherent porous structure, hydrophilic properties, and high stability in aqueous environments, has been utilized to create as support with enhanced surface hydrophilicity, reduced cross-linking, and preferential pathways for water molecules through selected layers of UiO-66-NH₂ nanoparticles. Building on these promising results, this research aims to thoroughly evaluate and characterize the synthesized catalyst UiO-66-NH₂@1-Chloro-2,3-epoxypropane@Cyclodextrin@Au-NPs. This catalyst is developed by combining UiO-66-NH₂ with epichlorohydrin (ECH) and cyclodextrin to cross-link and stabilize gold nanoparticles on the substrate. The goal is to design a remarkably effective and novel green catalyst: UiO-66-NH₂@1-Chloro-2,3-epoxypropane@Cyclodextrin@Au-NPs. This innovative catalyst has proven effective when employed in heterogeneous catalysis, demonstrating its flexibility in facilitating both C–C coupling and Carbonylative reactions.

Experimental section

The study utilized materials and reagents acquired from Merck and Sigma-Aldrich, which were utilized as received without purification. The synthesis processes described below were implemented.

Synthesis of UiO-66-NH₂@Epichlorohydrin@Cyclodextrin@Au-NPs catalyst

Synthesis of UiO-66-NH₂

Combine 2.05 g of 2-aminoterephthalic acid with 65 mL of dimethylformamide (DMF) in a three-necked flask and mix thoroughly. Dissolve 2.65 g of zirconium tetrachloride (ZrCl₄) in 55 mL of DMF and add it to the initial mixture. Introduce 2.5 mL of concentrated hydrochloric acid. Maintain an argon atmosphere and reflux the mixture at 130 °C for 24 h. Observe the solution as it transitions from deep purple to yellow, ultimately forming a clear yellow precipitate and powder³⁴.

Synthesis of UiO-66-NH₂@Epichlorohydrin (UiO-66-NH₂@1-Chloro-2,3-epoxypropane)

Stir 0.1 g of UiO-66-NH₂ in 50 mL of acetonitrile at room temperature for 30 min. Mix 0.5 mL of liquid epichlorohydrin with 0.5 mL of acetonitrile using a syringe, stirring for 5 min. Add this solution to the UiO-66-NH₂-acetonitrile mixture. Heat the combined solution to 65 °C and reflux for 24 h. Centrifuge the mixture at 9000 rpm to separate the solid. Wash the solid twice with fresh acetonitrile and dry it in an oven at 55 °C.

Synthesis of UiO-66-NH₂@1-Chloro-2,3-epoxypropane@Cyclodextrin

Prepare a solution of 0.5 g of cyclodextrin (CD) in 40 mL of anhydrous dimethyl sulfoxide (DMSO) with constant magnetic stirring. Stir 0.1 g of UiO-66-NH₂@1-Chloro-2,3-epoxypropane in 30 mL of DMSO for 30 min. Slowly add the cyclodextrin-DMSO solution dropwise to the UiO-66-NH₂@1-Chloro-2,3-epoxypropane solution. Gradually heat the mixture to 60 °C and reflux for 12 to 24 h. Isolate the product by centrifugation, rinse with dry DMSO, and dry it in an oven at 70 °C.

Synthesis of UiO-66-NH₂@1-Chloro-2,3-epoxypropane@Cyclodextrin@Au-nanoparticles

Dissolve 0.2 g of UiO-66-NH₂@1-Chloro-2,3-epoxypropane@Cyclodextrin in 35 mL of distilled water in a flask. In a separate container, dissolve 0.045 g of HAuCl₄ in 4 mL of distilled water and add it slowly to the flask while stirring vigorously to form Vessel A. Stir Vessel A at room temperature for 5 h. Dissolve 0.3 mL of hydrazine hydrate in 3 mL of distilled water to create Vessel B. Add Vessel B dropwise to Vessel A with continuous vigorous stirring. Stir the reaction mixture for an additional 24 h to ensure complete reduction of the gold nanoparticles (see Fig. 1)²⁹.

Results and discussion

To improve catalytic efficiency in chemical reactions, this study introduces a gold-based catalyst tailored for C–C coupling reactions. Therefore, UiO-66-NH₂ was utilized as a support for the heterogenization of Au-nanoparticles, owing to its high activity for PSM, substantial surface area, and robust structure. The PSM MOF was developed using a gradient strategy, whereby the organic compounds of epichlorohydrin were coordinated to the NH₂ groups of the organic MOF bonds. The amino NH₂ group of the MOF opens the epoxy ring of the

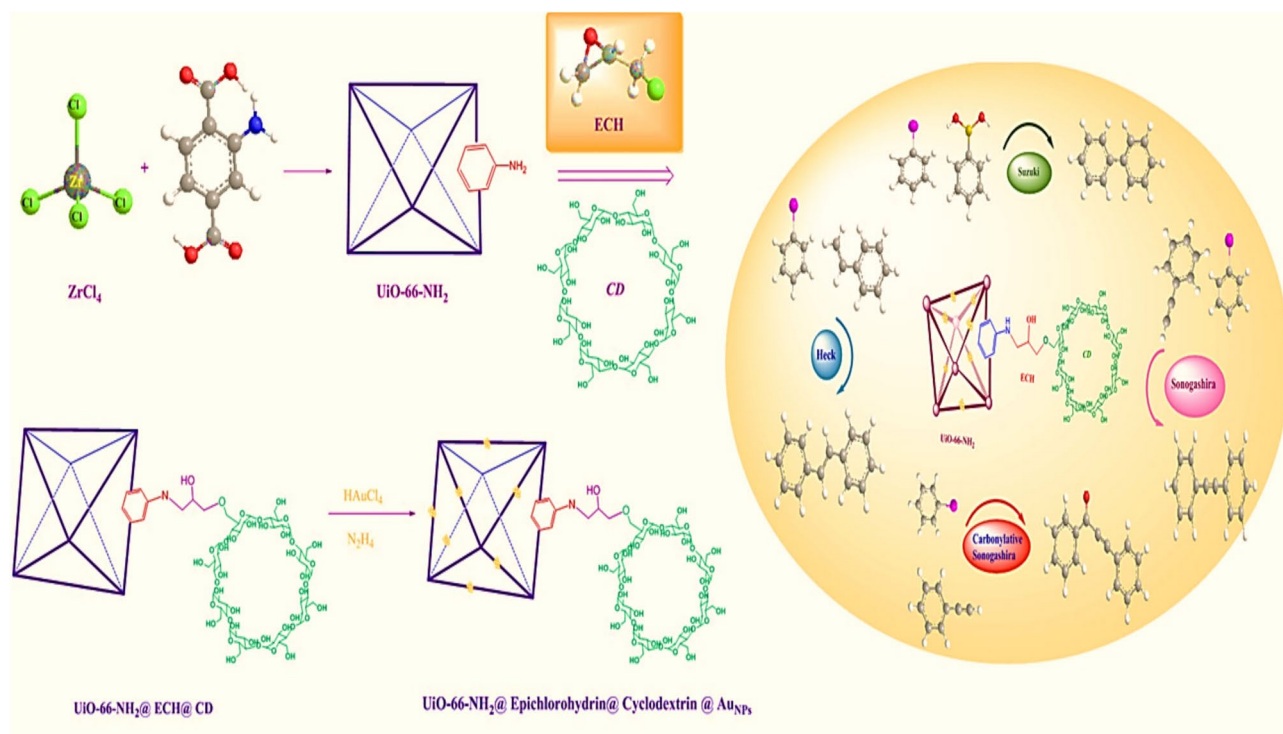


Fig. 1. The preparation of UiO-66-NH₂@Epichlorohydrin@Cyclodextrin@Au-NPs and application of catalyst in C–C couplings.

epichlorohydrin organic compound, resulting in the formation of UiO-66-NH₂/Epichlorohydrin. Subsequently, the chlorine group is eliminated from the opposite side through a reaction with the significant compound cyclodextrin, leading to the formation of UiO-66-NH₂/Epichlorohydrin/Cyclodextrin/Au-NPs. Its structure and performance were analyzed and validated by means of various techniques, e.g., FT-IR, XRD, BET, SEM, TGA, TEM, EDS, ICP, and mapping techniques. The loading of Au in the catalyst is thoroughly described, highlighting both the Au catalyst loading and the incorporation of Au nanoparticles into the catalyst, with both measurements derived from ICP analysis.

Fourier transform infrared spectrometer (FT-IR)

The FT-IR spectrum (Fig. 2) of the newly prepared UiO-66-NH₂@1-Chloro-2,3-epoxypropane@Cyclodextrin@Au-NPs reveals distinct features associated with the functionalization of UiO-66-NH₂ with epichlorohydrin, cyclodextrin, and gold nanoparticles. Absorption bands at approximately 3334 cm⁻¹ and 3289 cm⁻¹ are associated with NH₂ stretching vibrations. Peaks at 1644 cm⁻¹ and 1256 cm⁻¹ are related to N-H and C-H bending vibrations, respectively. The bands in the 3672–3678 cm⁻¹ range are related to the μ_3 -OH groups within the Zr₆ cluster. The C-H stretching vibrations are noted between 2800 and 13,100 cm⁻¹. Ester-related bands appear at 1730, 1705, and 1227 cm⁻¹. The significant absorption peaks at 1576, 1423, 1259, and 669 cm⁻¹ correspond to the stretching vibrations of C–O, C–C, C–Ar–N, and Zr/Hf–O bonds, respectively^{29,34}.

Transmission electron microscopy (TEM) analysis of UiO-66-NH₂@Epichlorohydrin@Cyclodextrin@Au-NPs catalyst

The TEM images of the UiO-66-NH₂@Epichlorohydrin@Cyclodextrin@Au-NPs catalyst provide detailed insights into the morphology of the catalyst. As depicted in Fig. 3, the TEM images reveal that the particle sizes range from 50 to 100 nm. The dark spots observed in the images indicate the well-dispersed gold nanoparticles (Au-NPs) on the surface of the modified MOF. The porous structure of the material is clearly visible and aligns with the particle size measurements obtained from the SEM images. The SEM images shown in Fig. 4 exhibit irregular, multi-stacked porous structures and a rough surface of UiO-66-NH₂. This roughness is a natural consequence of the PSM approach. Additionally, the Au nanoparticles, predominantly spherical, are observed with an average diameter ranging from 42.78 to 48.02 nm, as they are well-distributed on the UiO-66-NH₂ substrate.

X-ray diffraction (XRD)

Figure 5 presents the XRD pattern of the newly synthesized UiO-66-NH₂@Epichlorohydrin@Cyclodextrin@Au-NPs catalyst. The diffraction peaks at 7.2°, 8.4°, and 25.82° (2 θ) indicate the preservation of the internal structure of the MOF following the post-synthesis modification of UiO-66-NH₂¹¹⁸. Although there is a slight shift in the 2 θ values, which is a typical result of the synthesis process, the characteristic diffraction features of UiO-66-NH₂ are still evident. This shift confirms the successful retention of the MOF crystal structure throughout the synthesis. However, some interference is noted due to the overlap of peaks from cyclodextrin, which complicates the analysis. Despite this, the XRD patterns clearly show the characteristic peaks of gold nanoparticles (Au-NPs).

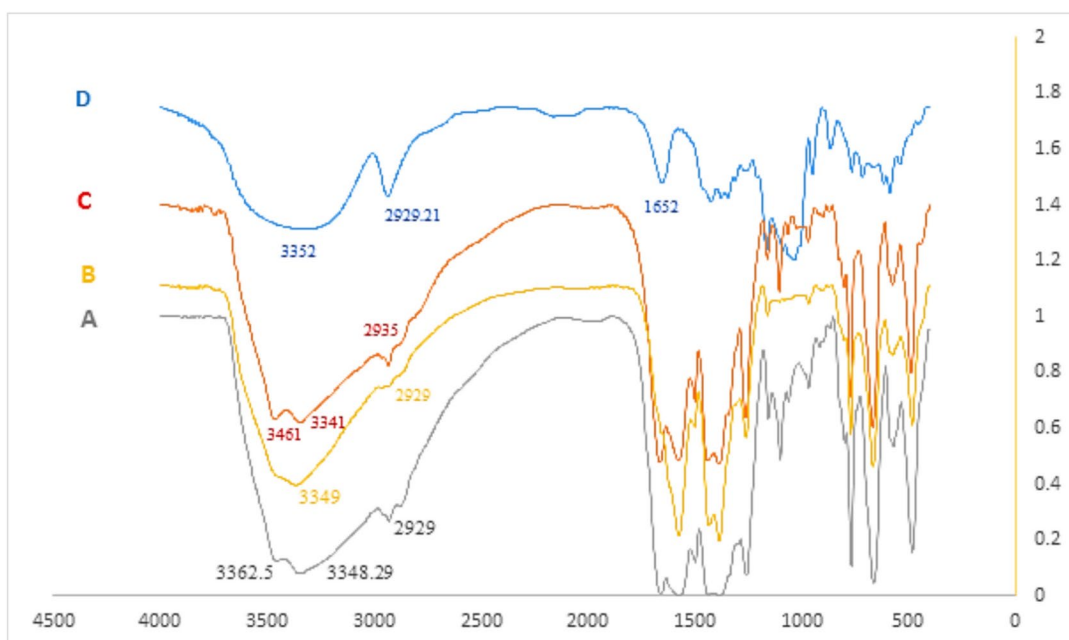


Fig. 2. IR spectra of (A) UiO-66-NH₂, (B) UiO-66-NH₂@Epichlorohydrin, (C) UiO-66-NH₂@Epichlorohydrin@Cyclodextrin, and (D) Cyclodextrin.

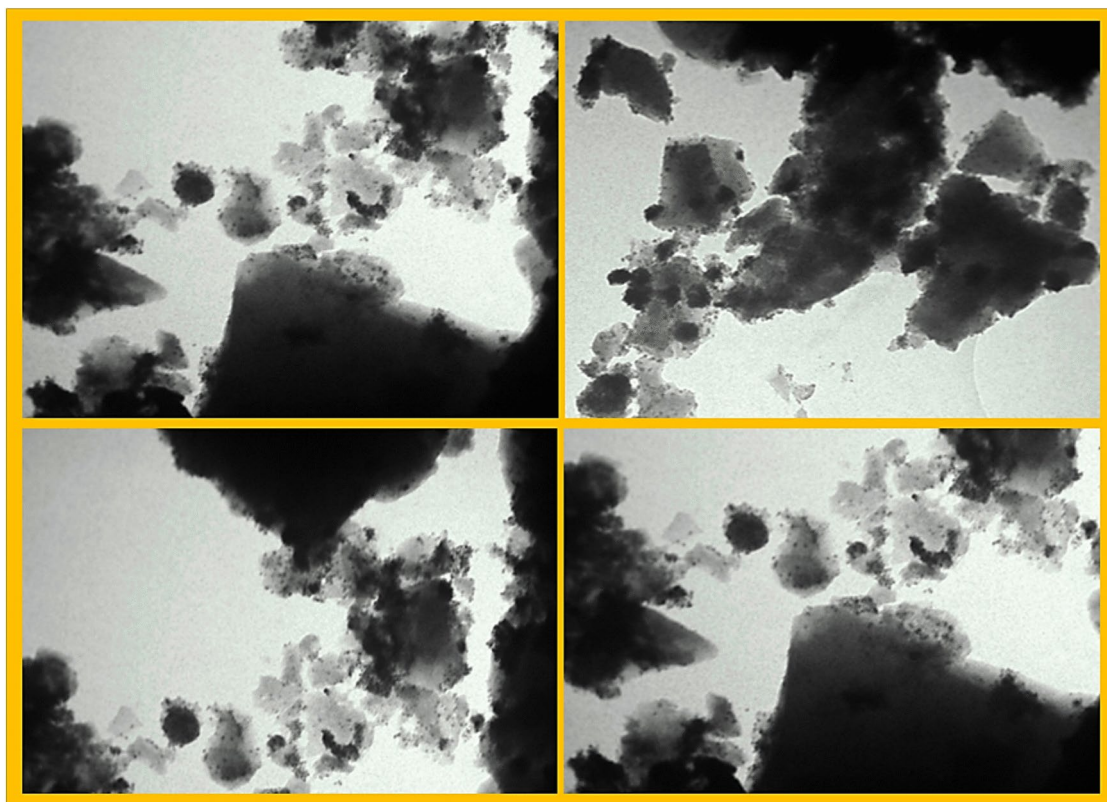


Fig. 3. TEM images of UiO-66-NH₂@Epichlorohydrin/Cyclodextrin/Au-NPs.

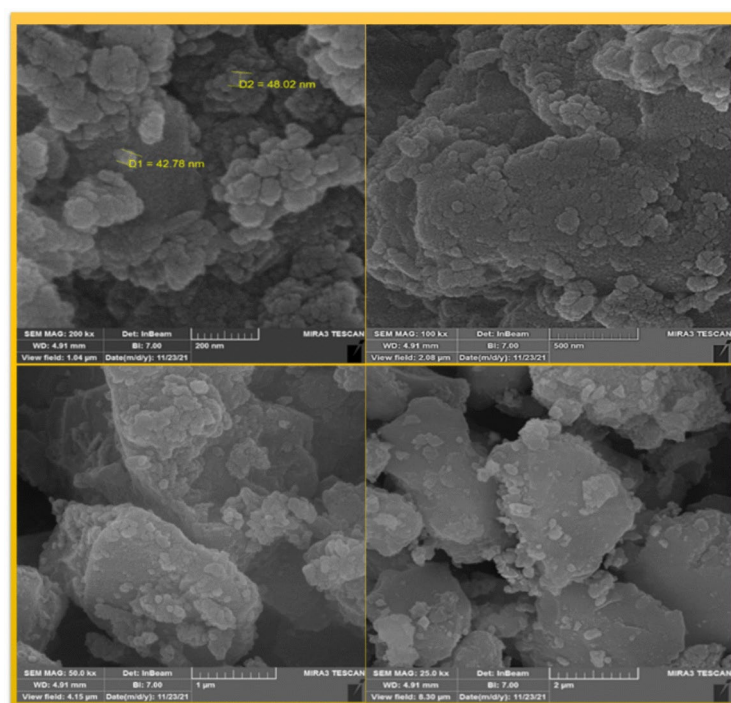


Fig. 4. SEM images of UiO-66-NH₂@Epichlorohydrin/Cyclodextrin/Au-NPs.

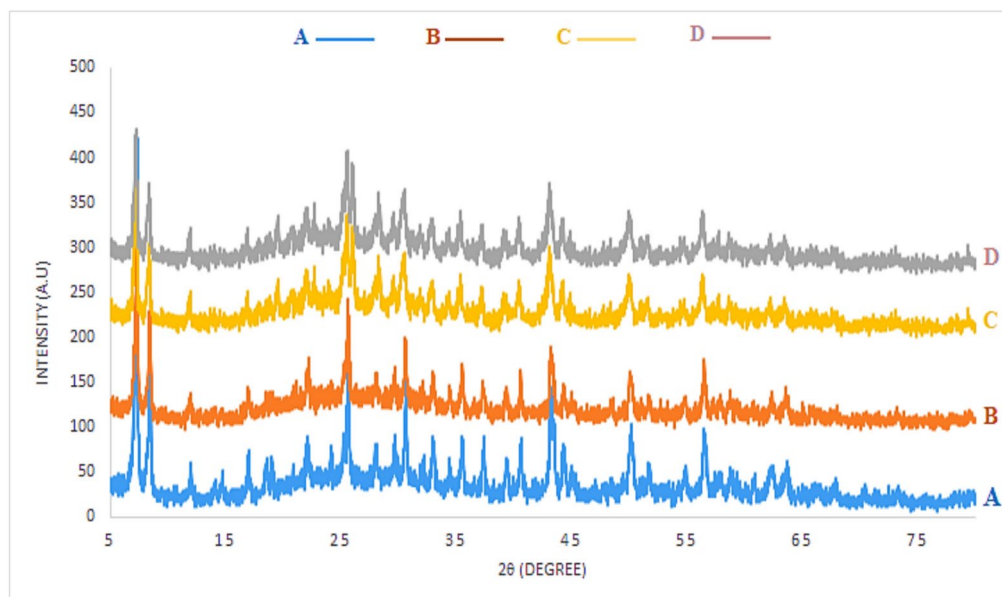


Fig. 5. The XRD pattern of the (A) UiO-66-NH₂ (B) UiO-66-NH₂@Epichlorohydrin (C) UiO-66-NH₂@Epichlorohydrin@Cyclodextrin and (D) UiO-66-NH₂@Epichlorohydrin@Cyclodextrin/Au-NPs.

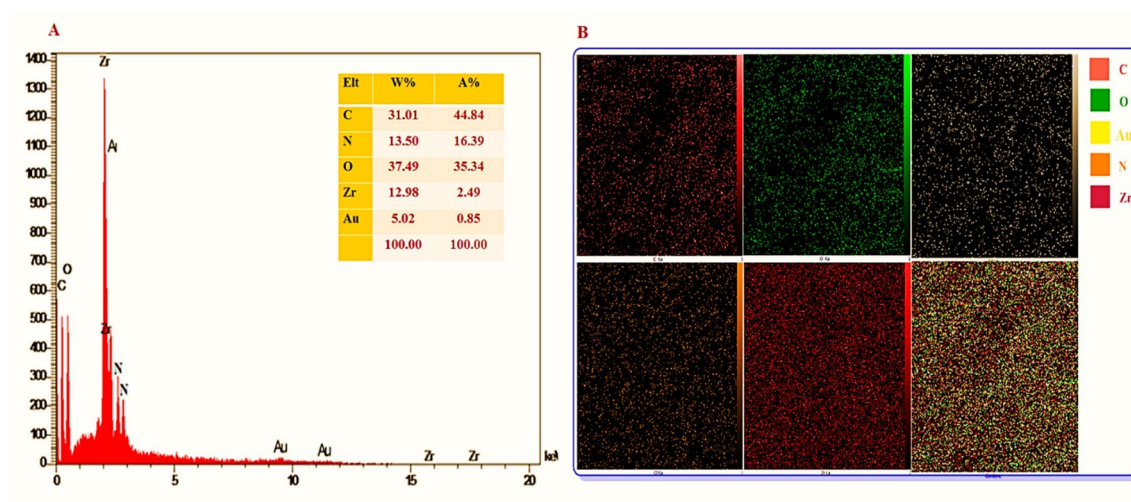


Fig. 6. (A) The EDS spectra and analysis for UiO-66-NH₂@Epichlorohydrin/Cyclodextrin/Au-NPs. (B) Mapping of carbon, oxygen, gold, nitrogen, zirconium and composite of all elements.

The reflections at 38.2°, 44.3°, 64.9°, and 77.8° (2θ) correspond to the standard Bragg reflections (111), (200), (220), and (311) of Au (JCPDS file: 04-0784)^{119,120}.

Figure 6 displays the elemental mapping analysis for the catalyst. This analysis reveals a uniform distribution of carbon (C), nitrogen (N), oxygen (O), zirconium (Zr), and gold (Au) throughout the catalytic structure. In addition, SEM–EDX mapping corroborates the existence of these elements, confirming the effective fabrication of the UiO-66-NH₂@Epichlorohydrin@Cyclodextrin@Au-NPs catalyst. Elemental analysis indicates that the gold loading in the catalyst is 5 wt%.

N₂ adsorption–desorption experiment

The porosity and surface area of the modified UiO-66-NH₂ MOF catalyst were assessed based on N₂ adsorption–desorption isotherm analysis (BET) at 77 K. As depicted in Fig. 7, the isotherm for the modified UiO-66-NH₂ at this temperature exhibits a Type I profile, indicative of substantial micro-porosity with an 820 cm³/g surface area. These findings validate the efficient modification of the UiO-66-NH₂ framework through PSM with epichlorohydrin and cyclodextrin, and the subsequent stabilization of gold nanoparticles. This process caused the surface area to shrink slightly, reflecting the modification of UiO-66-NH₂ structure (Fig. 7).

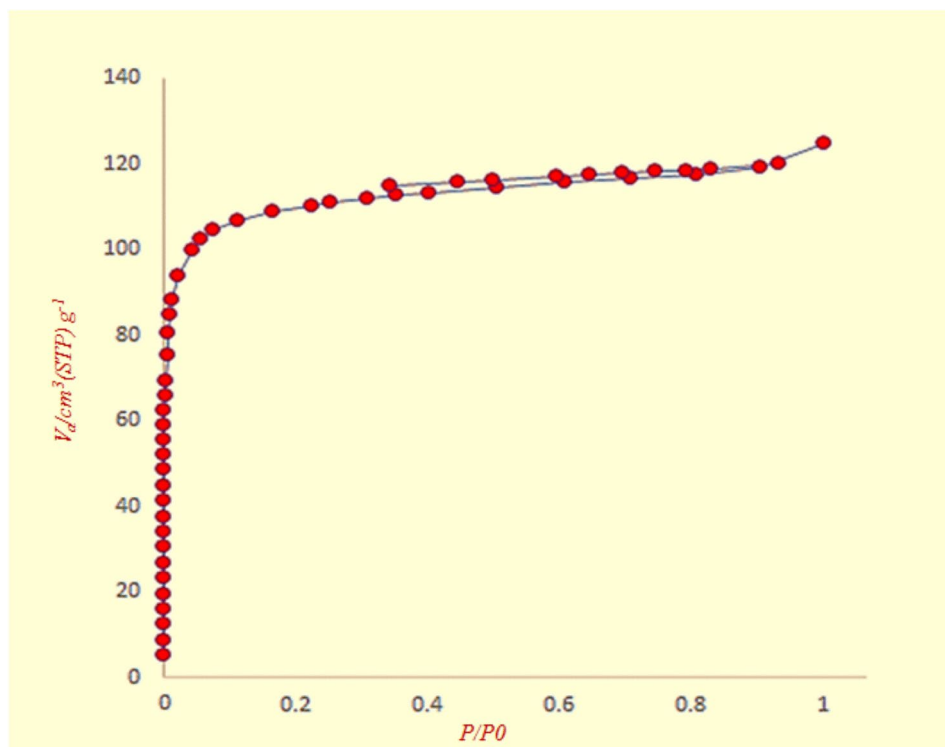


Fig. 7. The N_2 adsorption–desorption isotherm analysis (BET) of UiO-66- NH_2 and UiO-66- NH_2 @Epichlorohydrin@Cyclodextrin/Au-NPs.

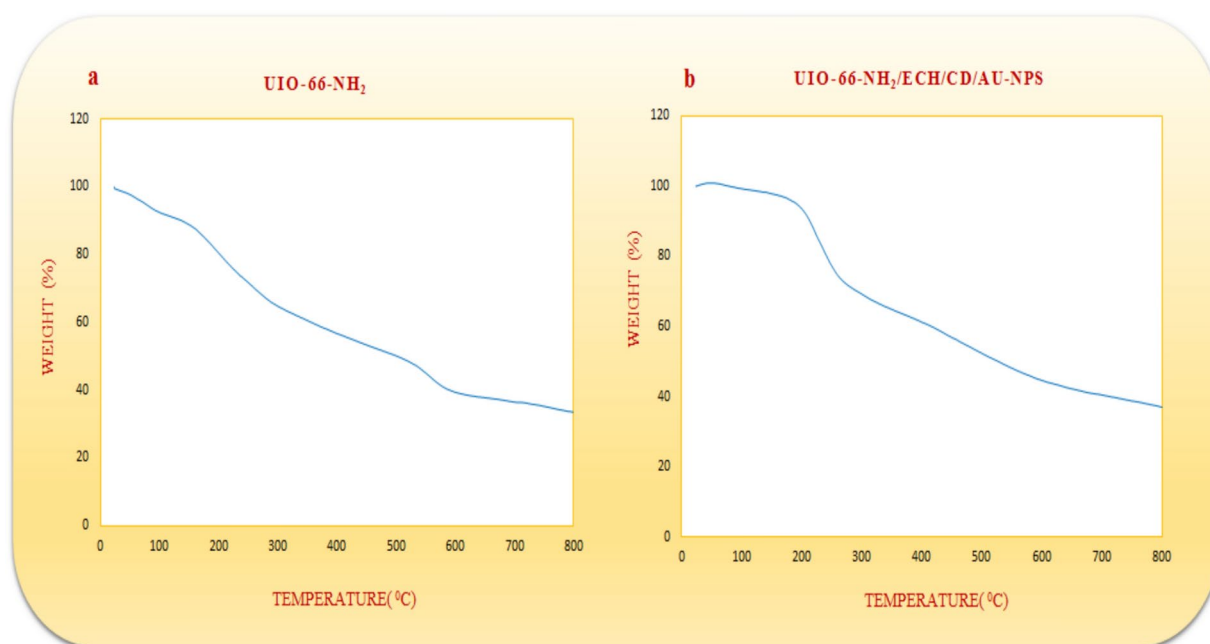


Fig. 8. DTA and TGA profiles of (a) UiO-66- NH_2 , and (b) UiO-66- NH_2 @Epichlorohydrin@Cyclodextrin@Au-NPs.

Thermogravimetric analysis (TGA)

Figure 8a presents the TGA and differential thermal analysis (DTA) of UiO-66- NH_2 . The TGA data reveal a two-phase weight reduction: the initial phase occurring at 90 °C, attributed to the elimination of adsorbed gases and coordinated hydroxyl groups from the zirconium clusters, and the second phase at 550 °C, associated

with the degradation of the framework, resulting in a final residue of 33.18% zirconium oxide. For UiO-66-NH₂ modified with epichlorohydrin and cyclodextrin (UiO-66-NH₂@epichlorohydrin@cyclodextrin), the first weight reduction phase occurs up to 280 °C, related to adsorbed gases and coordinated hydroxyl groups, while the second phase, between 550 and 750 °C, is due to framework decomposition. UiO-66-NH₂ modified with epichlorohydrin (UiO-66-NH₂@epichlorohydrin) and with cyclodextrin (UiO-66-NH₂@epichlorohydrin@cyclodextrin) show similar patterns, with final residues of 38.43% and 37.03%, respectively. These findings, depicted in Fig. 8a,b, demonstrate the enhanced thermal stability of the modified MOFs.

Plausible mechanism

According to the results of previously outlined findings, a mechanistic framework illustrating the likely sequence of occurrences is presented in (Fig. 9). In the case of Suzuki coupling, the process commences with the engagement of aryl boronic acids 1 and haloarenes 2 on the catalyst surface, leading to the formation of transient species I, which subsequently reorganizes to yield organometallic intermediate II¹²¹. The reaction in the presence of K₂CO₃ and water subsequently yields biaryl products 3, accompanied by byproducts KHCO₃, KX, and B(OH)₃ (Fig. 9A). In the Sonogashira coupling process, it is probable that the reaction advances via the chemisorption of terminal alkynes 4 and haloarenes 2 onto the catalyst surface, resulting in the formation of adsorbed species III. The molecules that have been adsorbed subsequently reorganize on the surface to generate intermediate IV (Fig. 9B). This latter intermediate, when reacted with K₂CO₃, yields the desired coupling products 5 along with KX and KHCO₃, while simultaneously regenerating the catalyst (Fig. 9)¹²².

UiO-66-NH₂@Epichlorohydrin@Cyclodextrin@Au-NPs has been engineered to enhance catalytic efficiency for a range of coupling reactions, such as Suzuki, Heck, Sonogashira C–C Coupling, and Carbonylative Sonogashira reactions. This catalyst operates effectively with H₂O as a green solvent in moderate conditions. Specifically, the Suzuki-Miyura cross-coupling reaction was selected as the model for optimization. This was achieved using the UiO-66-NH₂@Epichlorohydrin@Cyclodextrin@Au-NPs catalyst, with iodobenzene and phenylboronic acid, which notably enhanced the Suzuki reaction under mild conditions. Furthermore, the effects of various parameters, including temperature, solvent type, catalyst quantity, reaction time, and different bases, were evaluated and are summarized in Table 1. The development of the Suzuki reaction with the Au/UiO-66-NH₂ catalyst was analyzed to determine the optimal solvent among various options such as water, toluene, DMSO, DMF, CH₂Cl₂, MeCN, ethanol/water, ethanol, tetrahydrofuran, and NMP, with water demonstrating the most favorable results. Table 1 provides a comprehensive overview of how catalyst loading, temperature, reaction time, solvent type, and base selection impact the reaction parameters.

The optimal catalyst quantity was determined by evaluating the reaction progress at various catalyst loadings. As the catalyst amount increased from 10 to 25 mg, the efficiency of the reaction improved from 30 to 99%. This enhancement is attributed to the greater interaction rate between the substrates and the active sites of the catalyst. Consequently, a catalyst loading of 25 mg was found to be optimal for the Suzuki reaction. It was observed that no product was formed without the Au catalyst.

Moreover, the Suzuki reaction kinetics are influenced by reaction time and temperature. According to the data, increase in temperature from 25 to 80 °C indicates optimal result was achieved at 65 °C. More temperature increases did not result in higher reaction yields. Therefore, a temperature of 65 °C for 40 min was selected as the optimal condition for the reaction.

For the model reaction, water (H₂O) emerged as the most effective solvent, providing the highest yield. This is likely due to the enhanced solubility of phenylboronic acid and potassium carbonate in this solvent. Based on these findings, optimal yields were obtained with 25 mg of our catalyst, using water as the solvent and potassium carbonate as the base at 65 °C for 40 min.

The Carbonylative Sonogashira reaction was conducted using the Au-UiO-66-NH₂ catalyst, incorporating phenylacetylene, iodobenzene, acetic anhydride, a base, a ligand (10 mol percent), formic acid, and a solvent to synthesize the target compounds. As detailed in Table S3, optimal results were obtained with trimethylamine (Et₃N) as the base, toluene as the solvent, and 30 mg of UiO-66-NH₂@Epichlorohydrin/Cyclodextrin/Au-NPs, a modified version of Au-UiO-66-NH₂, at 60 °C for 7 h. These conditions for the reaction were identified as the most effective. Tables S1 and S2 present the optimization data for the Heck and Sonogashira reactions using the given catalyst.

In accordance with the prescribed methodology for the Heck reaction, iodobenzene was combined with styrene, while iodobenzene was paired with phenylboronic acid for the Suzuki reaction. The research findings indicate that the Heck reaction achieved the highest yield when conducted in water as the solvent, with potassium carbonate (K₂CO₃) serving as the base. The reaction was performed using 30 mg of UiO-66-NH₂@Epichlorohydrin/Cyclodextrin/Au-NPs as the catalyst at 80 °C for 90 min, resulting in optimal performance (see Table S1). This study found that using water as a green solvent, potassium carbonate (K₂CO₃) as a base, and 30 mg of UiO-66-NH₂@epichlorohydrin/cyclodextrin/Au-NPs as a catalyst, referred to as the Au-UiO-66-NH₂ catalyst, at 80 °C for 90 min led to maximum yield for the Heck reaction (see Table S1). The optimal conditions for the Sonogashira reaction, which involved 25 mg of the catalyst in water as the green solvent, K₂CO₃ as the base, 50 °C temperature, and a reaction time of 20 min, are detailed in Table S2. Similarly, the most effective conditions for the Suzuki reaction were found to be 25 mg of catalyst in water, with K₂CO₃, at 65 °C for 40 min (refer to Table 1).

After establishing the optimal Sonogashira conditions, the proposed method's generalizability was assessed by synthesizing various biphenyl derivatives from different precursors, such as aryl halides and terminal alkynes, using the catalyst prepared under optimal conditions (refer to Table 2). The results in the table demonstrate high yields of reaction products, irrespective of whether the aryl halides are *meta*-, *ortho*-, or *para*-substituted.

The Table 2 illustrates the Au/UiO-66-NH₂ catalyst excels in the Sonogashira coupling reaction, effectively handling bromine, iodine, and chlorine derivatives of aromatic compounds. The use of various aliphatic halides

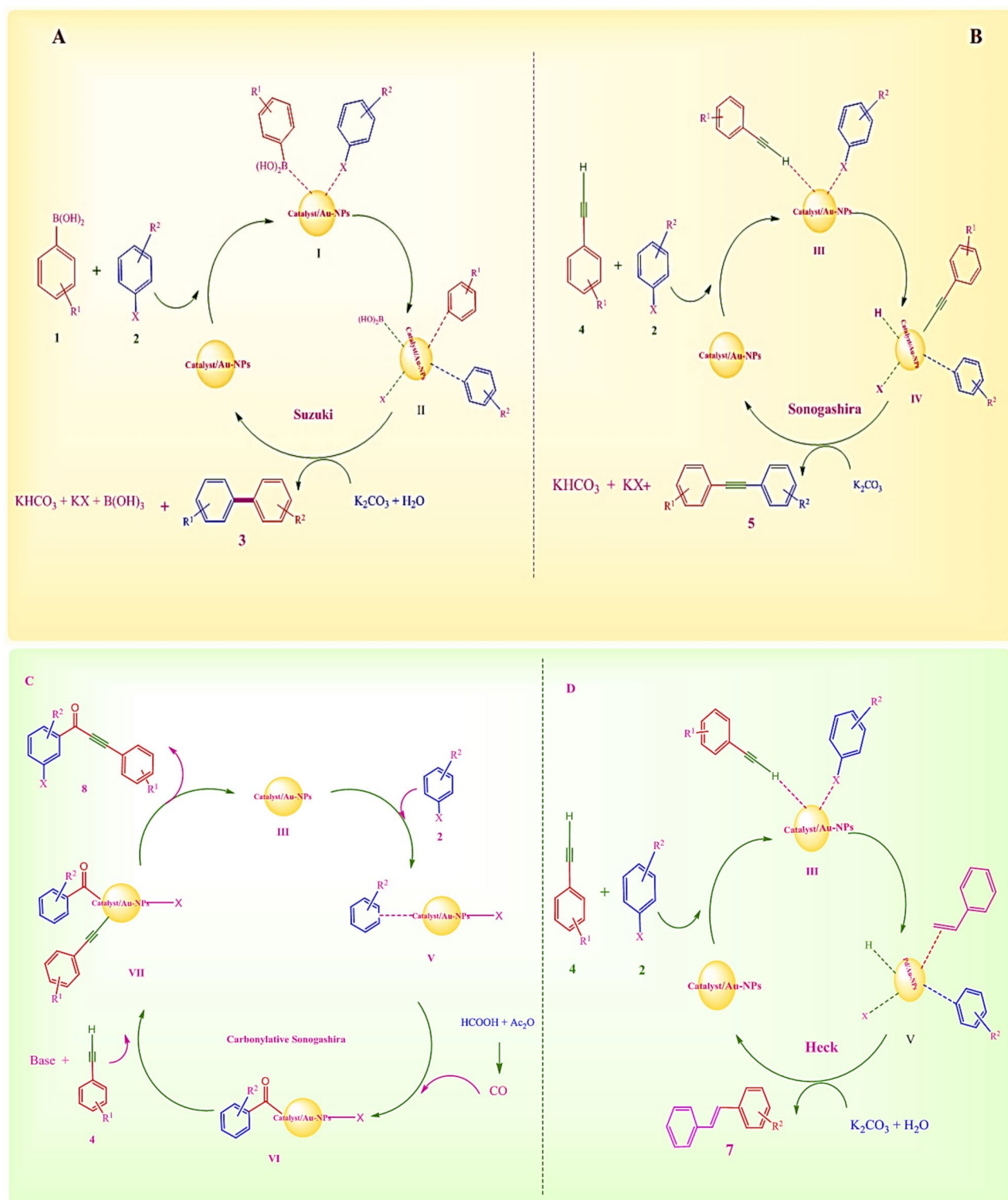


Fig. 9. Plausible mechanism in order to (A) Suzuki, (B) Sonogashira, (C) Carbonylative Sonogashira and (D) Heck coupling reaction by UiO-66-NH₂/Epichlorohydrin@Cyclodextrin/Au-NPs.

led to consistently high-quality products. Table 3 succinctly shows the results of the Sonogashira Carbonylative reaction with the Au-MOF catalyst. Further analysis of the Heck and Suzuki reactions is provided in Tables 4 and 5, respectively. The study demonstrates that UiO-66-NH₂/Epichlorohydrin/Cyclodextrin/Au-NPs serves as an excellent catalyst for coupling reactions, although certain products from the Sonogashira reaction yielded lower results compared to others (Table 2).


						
Entrance	Catalyst (mg)	Solvent	T (°C)	Base	Time (min)	Yield (%)
1	–	EtOH	25	K ₂ CO ₃	40	–
2	5	EtOH	35	K ₂ CO ₃	40	29
3	5	EtOH	80	K ₂ CO ₃	40	65
4	25	EtOH: H ₂ O (1: 1)	80	K ₂ CO ₃	40	98
5	30	EtOH: H ₂ O (1: 1)	80	K ₂ CO ₃	40	97
6	25	H ₂ O	70	K ₂ CO ₃	40	97
7	25	H ₂ O	65	K ₂ CO ₃	40	99
8	25	H ₂ O	60	K ₂ CO ₃	40	96
9	25	H ₂ O	55	K ₂ CO ₃	40	92
10	25	H ₂ O	60	KOH	40	90
11	25	H ₂ O	60	K ₃ PO ₄ ·3H ₂ O	40	78
12	25	H ₂ O	60	CH ₃ COONa	40	25
13	25	H ₂ O	60	Et ₃ N	40	50
14	25	H ₂ O	60	Piperidine	40	30
15	25	H ₂ O	60	Na ₂ CO ₃	40	68
16	25	DMSO	60	K ₂ CO ₃	40	–
17	25	DMF	60	K ₂ CO ₃	40	35
18	25	1,2-dichloromethane CH ₂ Cl ₂	40	K ₂ CO ₃	40	35
19	25	MeCN	60	K ₂ CO ₃	40	10
20	25	PhCH ₃	60	K ₂ CO ₃	40	30
21	25	NMP	60	K ₂ CO ₃	40	35
22	25	THF	60	K ₂ CO ₃	40	30

Table 1. Results from the optimization experiments for the Suzuki coupling reaction. Reaction conditions: 1 mmol of phenylboronic and acid 1 mmol of iodobenzene.

Once the optimal conditions were determined, the versatility of the reaction was assessed by synthesizing a range of biphenyl derivatives from different starting materials. This involved reacting various aryl halides and aryl boronic acids with the developed catalyst under the established optimal conditions, as detailed in Table 5. Results point out that the derivatives formed in the presence of aryl halide precursors were produced with high efficiency. The efficiency percentage was consistent regardless of whether the substituent positions on the aryl halide ring were ortho, meta, or para. Furthermore, the use of aliphatic halides also resulted in high-quality products. The proposed catalyst proved to be quite effective and versatile in catalyzing the Suzuki coupling process with iodine, chloro, and bromo derivatives of aromatic compounds.

The study further evaluated the effectiveness of the proposed method in the Sonogashira and Heck reactions, with the results detailed in Tables 3 and 4. This research demonstrated the effectiveness of UiO-66-NH₂@Epichlorohydrin@Cyclodextrin@Au-NPs in promoting these reactions, although the yields for certain products were somewhat lower in the Sonogashira reaction.

The effectiveness of the UiO-66-NH₂@Epichlorohydrin@Cyclodextrin@Au-NPs catalyst in the Suzuki cross-coupling reaction was evaluated against various other catalysts documented in prior studies, as visible in Table 5. As seen in Table 5, the catalyst in question demonstrates superior efficiency compared to the others. This superior performance can be attributed to the appropriate modifications made post-synthesis, specifically the use of epichlorohydrin and cyclodextrin compounds, which altered the electronic structure of UiO-66-NH₂. This modified structure enhances the capacity of Au NPs in the final composite to perform catalytic reactions and activities more effectively.

Recyclability

One of the key attributes of an effective catalyst is its reproducibility, which enables it to facilitate multiple iterations of the same reaction reliably. In this study, the proposed catalyst was evaluated for its performance in Cu-free Sonogashira, Carbonylative Sonogashira, Suzuki, and Heck reactions over 9 cycles. The catalyst consistently delivered high yields, ranging from 100 to 85%, as illustrated in Fig. 10. Importantly, there was no noticeable decline in performance after the first three cycles. The remarkable recyclability of the catalyst is due to the structural stability of UiO-66-NH₂ in aqueous conditions. Moreover, the modification process effectively prevents water from penetrating the MOF's pores, which significantly contributes to the catalyst's robustness and longevity.

The catalytic efficacy of UiO-66-NH₂@Epichlorohydrin/Cyclodextrin/Au-NPs in Sonogashira, Carbonylative Sonogashira, Heck and Suzuki reactions are benchmarked against other catalysts reported in the literature, as summarized respectively in Tables 2, 3, 4, and 5. The results suggest that the newly synthesized catalyst

Item	Arylhalide	Arylbronic acid	Product	Time (min)	Yield (%)
1				20	98
2				20	97
3				20	98
4				20	95
5				20	93
6				20	91
7				20	85
8				20	88
9				20	87
10				20	84
11				20	83
12				20	86
13				20	95
14				20	98
15				20	92
16				20	90
17				20	97
18				20	88
19				20	98
20				20	85

Table 2. The Sonogashira reaction using UiO-66-NH₂@Epichlorohydrin@Cyclodextrin@Au-NPs. Reaction conditions: 1 mmol of terminal alkyne, 3 mL of solvent, 1.2 mmol of aryl halide, and 2 mmol of base.

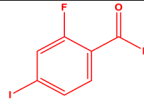
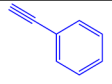
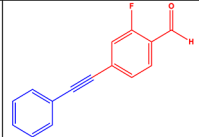
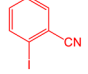
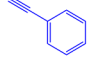
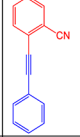
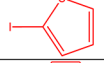
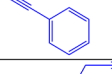
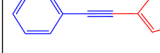
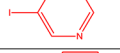

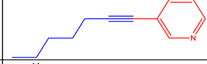
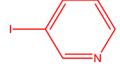
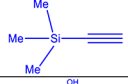
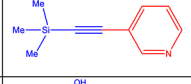
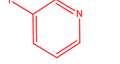
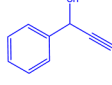
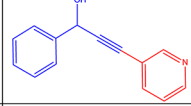
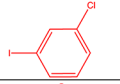
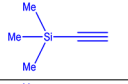
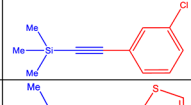
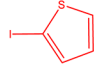
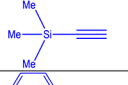
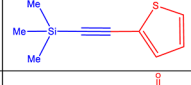
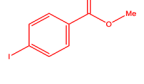
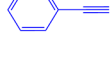
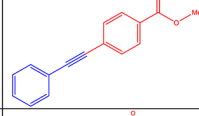
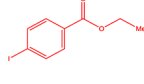
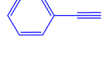
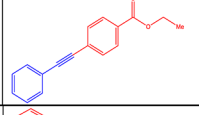
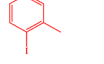
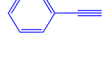
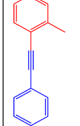
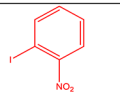
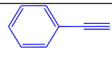
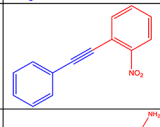
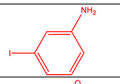
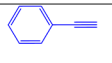
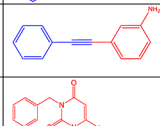
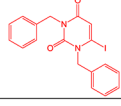
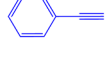
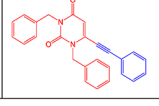
21				20	79
22				20	87
23				20	93
24				20	93
25				20	63
26				20	92
27				20	61
28				20	72
29				20	96
30				20	95
31				20	96
32				20	88
33				20	82
34				20	82

Table 2. (continued)

exhibits the most successful performance. This improved efficiency can be attributed to the post-synthesis conformational modifications using epichlorohydrin and beta-cyclodextrin, which enhance the UiO-66-NH₂ composite. The modified structure of UiO-66-NH₂ enhances the catalytic activity of the final composite by effectively immobilizing gold nanoparticles, leading to superior catalytic performance.

Results for the heterogeneous catalyst

In the model reaction, 1 mmol of phenylboronic acid was reacted with 1 mmol of iodobenzene in the presence of UiO-66-NH₂@Epichlorohydrin/Cyclodextrin/Au-NPs. The yield of the product was 99%. The highest efficiency was observed with 25 mg of the given catalyst, using water as the green solvent at 50 °C under 25 min.

In subsequent experiments, the same reaction setup was employed to assess the catalyst's heterogeneous properties, with the reaction conditions kept constant. Midway through the reaction, the catalyst was extracted

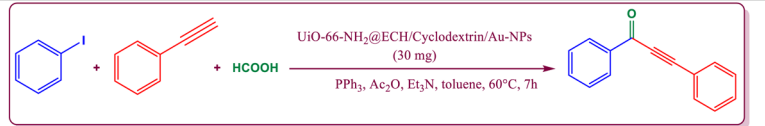
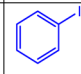
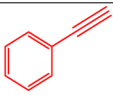
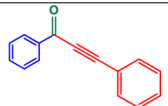
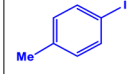
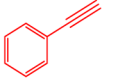
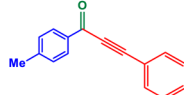
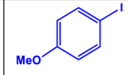
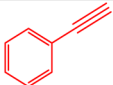
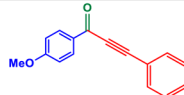
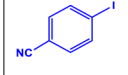
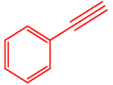
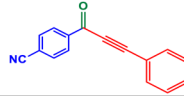
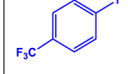
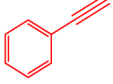
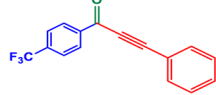
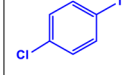
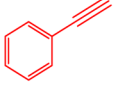
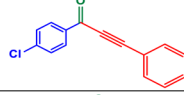
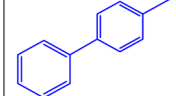
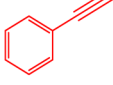
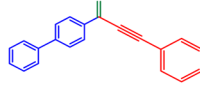
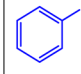
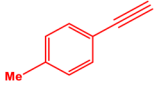
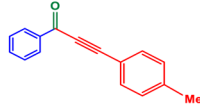
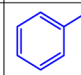
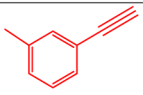
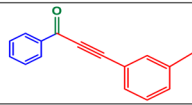
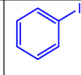
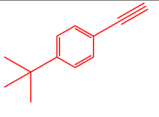
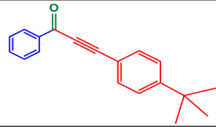
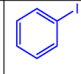
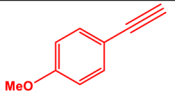
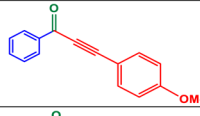
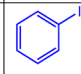
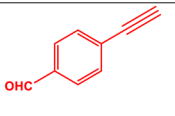
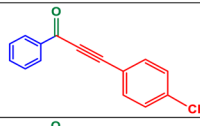
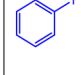
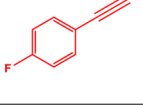
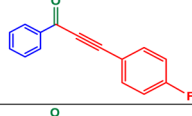
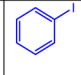
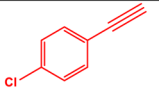
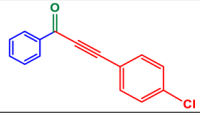
					
Item	Arylhalide	Arylbronc acid	Product	Time (h)	Yield (%)
1				7	96
2				7	97
3				7	94
4				7	59
5				7	61
6				7	56
7				7	79
8				7	96
9				7	98
10				7	85
11				7	91
12				7	75
13				7	84
14				7	89

Table 3. Organic compounds fabricated via the Carbonylative Sonogashira reaction.

Reaction Conditions: aryl acetylenes (0.4 mmol), aryl iodides (0.2 mmol), suggested catalyst UiO-66-NH₂@ECH/Cyclodextrin/Au-NPs (30 mg), PPh₃ (10 mol%), Et₃N (3 mmol), HCOOH (2.0 mmol), Acetic anhydride (Ac₂O) (2 mmol), toluene (2.0 ml), 50 °C, 8 h.

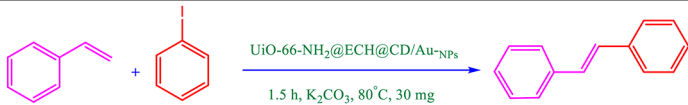
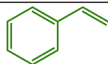
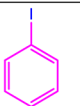
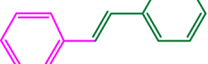
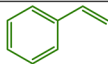
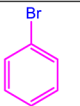
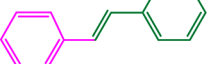
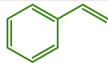
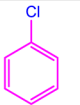
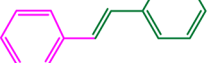
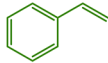
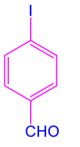
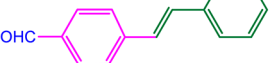
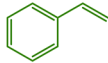
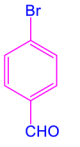
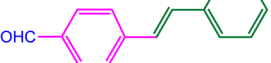
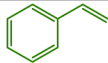
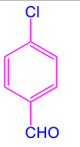
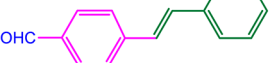
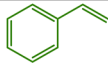
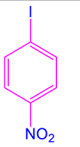
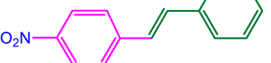
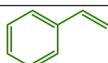
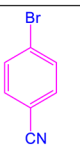
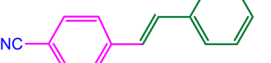
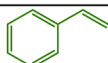
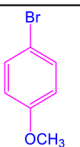
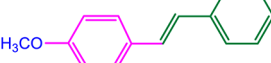
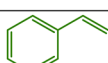
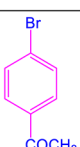
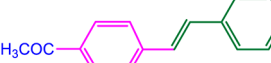
					
Entry	Alkene	Aryl halide	Product	Time (h)	Yield (%)
1				1.5	98
2				1.5	83
3				1.5	70
4				1.5	98
5				1.5	93
6				1.5	82
7				1.5	98
8				1.5	97
9				1.5	92
10				1.5	96

Table 4. Organic compounds fabricated via the Heck reaction in favorable conditions.

Reaction conditions: 1 mmol of aryl halide, 1 mmol of terminal alkyne, 2 mmol of base, 3 mL of solvent.

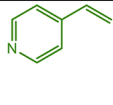
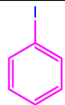
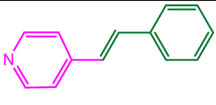
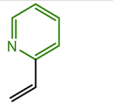
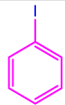
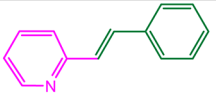
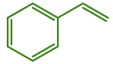
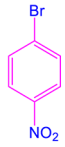
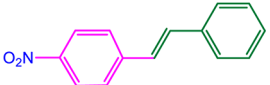
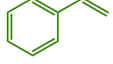
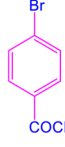
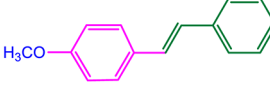
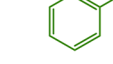

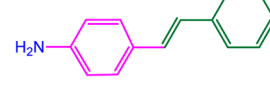
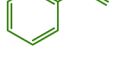
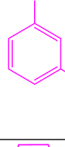
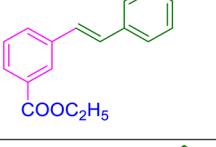
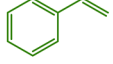
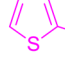
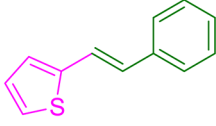
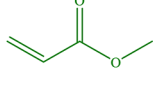
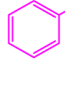
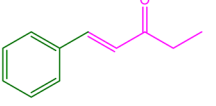
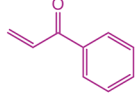

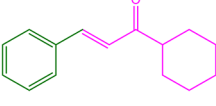
11				1.5	93
12				1.5	89
13				1.5	96
14				1.5	82
15				1.5	84
16				1.5	90
17				1.5	87
18				1.5	90
19				1.5	92

Table 4. (continued)

from the setup and the reaction was allowed to proceed for extra 100 min without it. After 25 min, the results showed that Container 1, which retained the catalyst, had a product yield of 99%. In contrast, Container 2, from which the catalyst was removed, yielded only 50% of the product, with no further increase in product yield observed (Tables 6, 7).

Table 8 illustrates a comparison of the catalytic efficacy of UiO-66-NH₂@Epichlorohydrin/Cyclodextrin@AuNPs alongside various catalysts documented in the literature for the purpose of Suzuki process. The data demonstrates that our suggested catalyst achieves one of the most significant yields recorded to date. This result may be attributed to the precise alteration of the electronic structure of UiO-66-NH₂ via a post-synthesis modification procedure utilizing nitrogen-rich ligands. The inclusion of Epichlorohydrin and Cyclodextrin alters the electronic structure of UiO-66-NH₂, consequently resulting in an enhancement and improving of the catalytic performance of gold nanoparticles within the final composite.

Results of inductively coupled plasma-optical emission spectroscopy (ICP-OES)

The ICP-OES analysis revealed that the Au loading of the new catalyst was 0.89%. The analysis of the recovered catalyst demonstrated minimal gold (Au) leaching, with a decrease of less than 0.02% after nine cycles of use. Additionally, the ICP analysis indicated that the Au loading of the created catalyst was 0.89%. After seven cycles

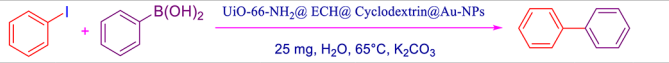
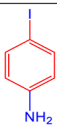
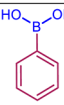
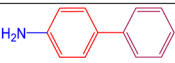


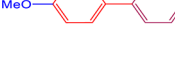
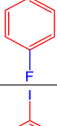


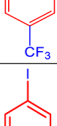
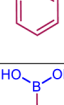

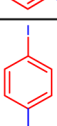
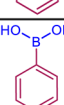

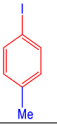
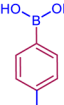
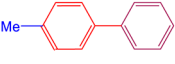
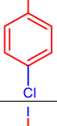
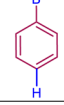

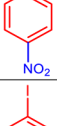



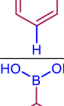

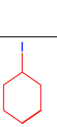
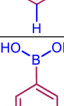
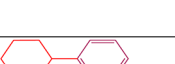
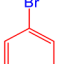
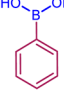

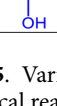
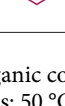
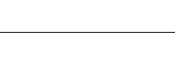



					
Entry	Aryl halide	Aryl boronic acid	Product	Time (min)	Yield (%)
1				40	97
2				40	97
3				40	99
4				40	99
5				40	77
6				40	92
7				40	95
8				40	99
9				40	98
10				40	99
11				40	92
12				40	99
13				40	76

Table 5. Various desired organic compounds fabricated using Suzuki coupling reaction. Chemical reaction conditions: 50 °C, H₂O, K₂CO₃, 1.1 mmol of aryl boronic acid, and 1 mmol of aryl halide.

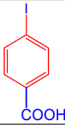
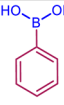

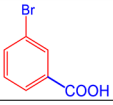
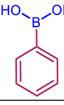
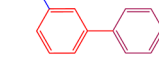
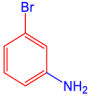
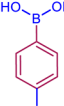

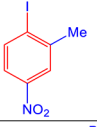
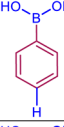

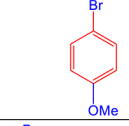
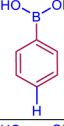

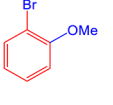
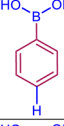

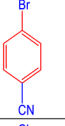
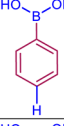

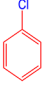
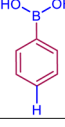

14				40	95
15				40	90
16				40	98
17				40	96
18				40	98
19				40	97
20				40	95
21				40	94

Table 5. (continued)

of use, there was a minor decrease in gold (Au) leaching, less than 0.05%. The Au loading of the catalyst is detailed in Table 9, which presents the Au catalyst loading and the loading of Au nanoparticles in the catalyst, both obtained from ICP analysis.

Combined catalytic reaction procedures

In a series of catalytic reactions, varying procedures were employed using a UiO-66-NH₂@Epichlorohydrin/Cyclodextrin/Au-NPs catalyst under similar conditions.

For the Suzuki reaction, 1.1 mmol of aryl boronic acid and 1 mmol of aryl halide were mixed in a 10 mL round-bottom flask with 3 mL of distilled water. To this mixture, 25 mg of the catalyst and 2 mmol of K₂CO₃ were added. The mixture was stirred and heated to 65 °C as specified in Table 5, and its progress was monitored by thin-layer chromatography (TLC) using an n-hexane/ethyl acetate (7:3) solvent system. Next, the mixture was allowed to cool to 25 °C, after which the catalyst was removed through filtration. Diethyl acetate was used to extract the organic phase. The resulting extract was then dried with magnesium sulfate (MgSO₄) and filtered to achieve purification. Purification of the crude product was achieved through column chromatography on silica gel with an n-hexane/ethyl acetate (7:1) solvent system. The final product was characterized by FT-IR, NMR spectroscopy, and melting point analysis, as detailed in the Supporting Information.

In the Sonogashira reaction, 1 mmol of halo benzene and 1.2 mmol of acetylene were mixed with 3 mL of distilled water in a reaction flask. The reaction was catalyzed by 25 mg of UiO-66-NH₂@Epichlorohydrin/Cyclodextrin/Au-NPs and 2 mmol of K₂CO₃. The mixture was heated to 50 °C and stirred as detailed in Table 2. Progress was tracked using TLC with an n-hexane/ethyl acetate (8:1) solvent system. After completion, the catalyst was filtered out, washed with ethanol, and dried at 60 °C. The organic phase was extracted with diethyl ether (Et₂O), and the crude product was purified using column chromatography on silica gel with an n-hexane/ethyl acetate (9:1) solvent system. Product characterization was conducted via FT-IR, NMR spectroscopy, and melting point analysis, as specified in the Supporting Information.

For the Carbonylative Sonogashira reaction, 30 mg of UiO-66-NH₂@Epichlorohydrin/Cyclodextrin/Au-NPs and 10 mol% PPh₃ were combined in a 15 mL desiccator tube, which was subjected to repeated evacuations and nitrogen purges. A mixture of 2.0 mL toluene, 1.0 mmol Et₃N, 0.4 mmol alkyne, and 0.2 mmol aryl iodide was

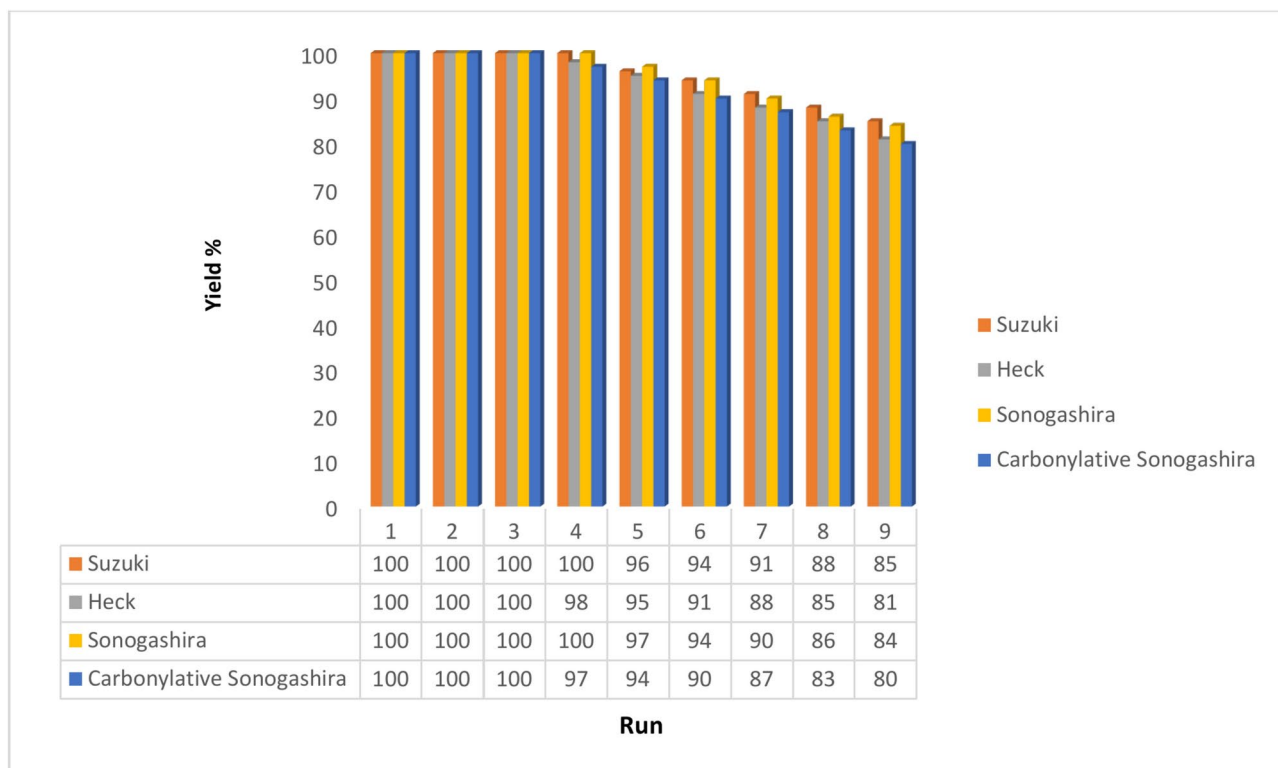


Fig. 10. Recyclability of the UiO-66-NH₂@Epichlorohydrin/Cyclodextrin/Au-NPs catalyst.

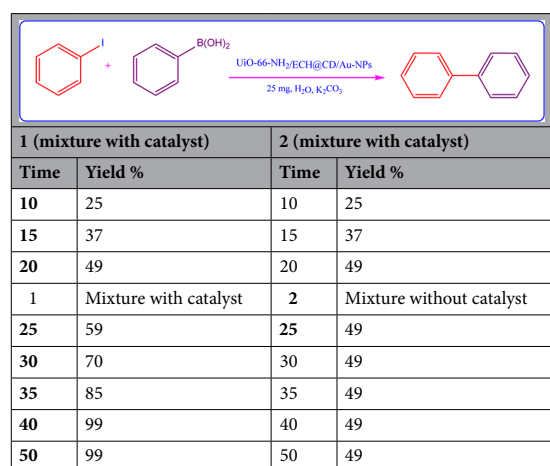
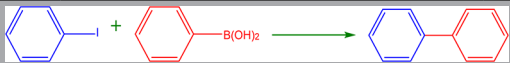


Table 6. Results for proving the heterogeneous catalyst. Significant values are in bold. Conditions: 1 mmol of terminal alkyne, 1.1 mmol of aryl halide, 2 mmol of base, and 3 mL of solvent.

Entrance	Catalyst	Yield%	Time (min)	Au (mmol g ⁻¹)	Leaching Au (mmol g ⁻¹)
1	UiO-66-NH ₂ @Epichlorohydrin/Cyclodextrin/Au-NPs	99	20	0.085	0.009
2	UiO-66-NH ₂ @Epichlorohydrin/Au-NPs	85	20	0.079	0.02
3	UiO-66-NH ₂ @Au-NPs	81	20	0.069	0.025

Table 7. Comparison of catalytic performance for the Sonogashira reaction using the synthesized catalyst versus alternative catalysts.



Entry	Catalyst	Reaction condition	Yield (%)	Time (h)	References
1	Pd@Mag-MSN (1)	K ₂ CO ₃ , CH ₂ Cl ₂ , 80 °C	85	6	123
2	Xerogel g1-MNPs (1)	Na ₂ CO ₃ , CH ₃ OH, 60 °C	99	2	124
3	Pd/NiFe ₂ O ₄ (0.1)	Na ₂ CO ₃ , DMF, 90 °C	50	2	125
4	Pd-Fe ₃ O ₄ (1)	K ₂ CO ₃ , DME: H ₂ O 3: 1, reflux	71	24	126
5	C/Co@PNIPAM-PPh ₂ -Pd (3)	K ₂ CO ₃ , toluene: H ₂ O 2: 1, 85 °C	99	16	127
6	Co@C@Pd (1.1)	Na ₂ CO ₃ , THF: H ₂ O 1: 2, 65 °C	96	2	128
7	Pd/Fe ₃ O ₄ @C (0.3)	K ₂ CO ₃ , EtOH, reflux	100	1	129
8	Pd@Fe ₃ O ₄ (0.816)	K ₃ PO ₄ , CH ₃ OH, 40–65 °C	90	18	130
9	Fe ₃ O ₄ @PUNP ^a -Pd (0.1)	K ₂ CO ₃ , H ₂ O, 90 °C	98	1	131
10	GA-FSNP@Pd (0.28)	K ₂ CO ₃ , solvent free, 90 °C	92	0.25	132
11	Pd-IPG (0.1)	NaOH, EtOH: H ₂ O, 60 °C	99	1	133
12	GO/NHC-Pd (1)	Na ₃ PO ₄ ·12H ₂ O, H ₂ O, 100 °C	91.6	6	134
13	Pd NPs on polymer (0.08)	K ₂ CO ₃ , H ₂ O, 25–100 °C	83	5	135
14	Pd-HoMOF (0.4)	KOH, DMF, 100 °C	99	1	136
15	(Pd (II)-NHCs) _n @nSiO ₂ (0.27)	K ₂ CO ₃ , DMF: H ₂ O (2:1), 60 °C	97	6 min	137
16	Pd (II)-NiFe ₂ O ₄ (0.5)	K ₂ CO ₃ , EtOH: H ₂ O, 80 °C	96	3	125
17	GO-CPTMS@Pd-TKHPP (10)	K ₂ CO ₃ , EtOH: H ₂ O, 80 °C	99	15 min	138
18	UiO-66-NH ₂ @Epichlorohydrin/Cyclodextrin/Au-NPs	H ₂ O, K ₂ CO ₃ , 60 °C	99	60 min	This study

Table 8. Comparative catalytic performance of the synthesized catalyst in the Suzuki reaction relative to existing literature reports.

Entrance	Catalyst	Au (mol%)
1	Order 1	0.89
2	Order 2	0.88
3	Order 3	0.88
4	Order 4	0.87
5	Order 5	0.86
6	Order 6	0.85
7	Order 7	0.84
8	Order 8	0.82
9	Order 9	0.82

Table 9. Au loading.

added via syringe. A separate solution of 2.0 mmol acetic anhydride and 2.0 mmol Et₃N was then introduced. The blend underwent stirring at 60 °C for a duration of 8 h, followed by filtration. Subsequently, the solution was subjected to concentration under vacuum at 60 °C. The resulting crude product was refined via column chromatography on silica gel, employing a solvent system of 95:5 petroleum ether and ethyl acetate.

Lastly, in the Heck reaction, 1 mmol of aryl halide, 1.1 mmol of olefin, 2 mmol of K₂CO₃, 3 mL of distilled water, and 30 mg of UiO-66-NH₂@Epichlorohydrin/CD/Au-NPs catalyst was combined in a 10 mL round-bottom flask. The mixture was heated to 80 °C under the conditions specified in Table 4. Upon completion, the catalyst was removed by centrifugation, and the solution was cooled. Organic compounds were extracted with ethyl acetate, and the solvent was evaporated. The residue was dried using MgSO₄, and the crude products were purified by column chromatography on silica gel with an n-hexane/ethyl acetate (9:1) solvent system. The final products were identified using FT-IR, NMR spectroscopy, and melting point analysis, as detailed in the Supporting Information.

Conclusions

In this research study, UiO-66-NH₂ was used as a support for the heterogenization of gold nanoparticles due to its high activity for PSM, as well as its significant surface area and robust structure. In this synthesis, which involves functionalization of MOF UiO-66-NH₂ via PSM cross-linked with epichlorohydrin (ECH) and cyclodextrin, gold nanoparticles were subsequently anchored onto this modified framework, resulting in the aforementioned novel catalyst, which led to the formation of UiO-66-NH₂/Epichlorohydrin/Cyclodextrin/Au-NPs. In this efficient strategy, cyclodextrin incorporation into UiO-66-NH₂ metal–organic frameworks (MOFs) was developed under milder preparation conditions, without compromising the framework's ability to adsorb

and store guest molecules. The process of bridging cyclodextrin with MOFs presents significant challenges. Cross-linked polymers, which are produced by (co)polymerization of cyclodextrin molecules and coupling agents in an alkaline medium, have attracted much attention due to their simple synthesis, high adsorption properties, and specific selectivity. Among the various methods, chemical cross-linking with epichlorohydrin is particularly noteworthy for creating a water-insoluble cyclodextrin network, which is advantageous for environmental applications. Furthermore, the properties were characterized and evaluated through analysis performed using FT-IR, XRD, BET, SEM, TGA, TEM, EDS, ICP, and mapping techniques. The proposed composite is used to facilitate C–C coupling reactions, including Suzuki, Heck, and Sonogashira, C–C reactions as well as Sonogashira carbonylation reactions, showing exceptional performance under mild conditions. As a result, considering the inherent stability of UiO-66-NH₂ MOF and the additional stability provided by PSM, the proposed catalyst showed outstanding recycling capabilities. Furthermore, the proposed catalyst showed the potential to be reused up to 9 times. Eventually, the techniques utilized for the heterogenization tests discussed in the preceding section, the outcomes achieved a product with high efficiency.

Data availability

All data generated or analyzed during this study are included in this published article (and its Supplementary information).

Received: 28 November 2024; Accepted: 7 April 2025

Published online: 25 April 2025

References

- Wasiak, T. & Janas, D. Nanowires as a versatile catalytic platform for facilitating chemical transformations. *J. Alloys Compd.* **892**, 162158. <https://doi.org/10.1016/j.jallcom.2021.162158> (2022).
- Fihri, A., Bouhrara, M., Nekouishahraki, B., Basset, J.-M. & Polshettiwar, V. Nanocatalysts for Suzuki cross-coupling reactions. *Chem. Soc. Rev.* **40**(10), 5181–5203. <https://doi.org/10.1016/j.jallcom.2021.162158> (2011).
- Primo, A. & Garcia, H. Supported gold nanoparticles as heterogeneous catalysts for CC coupling reactions. *Gold Catal. Prep., Charact., Appl.* **389**, 9780429083860 (2016).
- Li, G. & Jin, R. Catalysis by gold nanoparticles: Carbon-carbon coupling reaction. *Nanotechnol. Rev.* **2**(5), 529–545 (2013).
- Sankar, M. et al. Role of the support in the gold-containing nanoparticles as heterogenous catalysts. *Chem. Rev.* **120**(8), 3890–3938. <https://doi.org/10.1021/acs.chemrev.9b00662> (2020).
- Liu, K., Li, N., Ning, Y., Zhu, C. & Xie, J. Gold-catalyzed oxidative biaryl cross-coupling of organometallics. *Chem* **5**(10), 2718–2730. <https://doi.org/10.1016/j.chempr.2019.07.023> (2019).
- Ambehave, S. B. & Patil, N. T. Gold-catalyzed cross-coupling and 1, 2-difunctionalization reactions: A personal account. *Synlett* **34**(07), 698–708. <https://doi.org/10.1055/a-1893-7653> (2023).
- Chen, G. & Xu, B. Gold catalyzed C–O cross coupling reactions of aryl iodides with silver carboxylates. *Org. Lett.* **25**(34), 6334–6339. <https://doi.org/10.1021/acs.orglett.3c02254> (2023).
- Garcia, P., Malacria, M., Aubert, C., Gandon, V. & Fensterbank, L. Gold-catalyzed cross-couplings: New opportunities for C–C bond formation. *ChemCatChem* **2**(5), 493–497. <https://doi.org/10.1002/cctc.200900319> (2010).
- Li, X. et al. Unveiling the effects of linker substitution in Suzuki coupling with palladium nanoparticles in metal-organic frameworks. *Catal. Lett.* **148**, 940–945. <https://doi.org/10.1007/s10562-017-2289-9> (2018).
- Yuan, B., Pan, Y., Li, Y., Yin, B. & Jiang, H. A highly active heterogeneous palladium catalyst for the Suzuki–Miyaura and ullmann coupling reactions of aryl chlorides in aqueous media. *Angew. Chem. Int. Ed.* **49**(24), 4054–4058. <https://doi.org/10.1002/anie.201000576> (2010).
- Widegren, J. A. & Finke, R. G. A review of the problem of distinguishing true homogeneous catalysis from soluble or other metal-particle heterogeneous catalysis under reducing conditions. *J. Mol. Catal. A Chem.* **198**(1–2), 317–341. [https://doi.org/10.1016/S1381-1169\(02\)00728-8](https://doi.org/10.1016/S1381-1169(02)00728-8) (2003).
- Chouhan, A. S. & Sarma, A. K. Modern heterogeneous catalysts for biodiesel production: A comprehensive review. *Renew. Sust. Energ. Rev.* **15**(9), 4378–4399. <https://doi.org/10.1016/j.rser.2011.07.112> (2011).
- De Lima, A. L., Ronconi, C. M. & Mota, C. J. Heterogeneous basic catalysts for biodiesel production. *Catal. Sci. Technol.* **6**(9), 2877–2891. <https://doi.org/10.1039/C5CY01989C> (2016).
- Di Serio, M. et al. From homogeneous to heterogeneous catalysts in biodiesel production. *Ind. Eng. Chem. Res.* **46**(20), 6379–6384. <https://doi.org/10.1021/ie070663q> (2007).
- Chaturvedi, S., Dave, P. N. & Shah, N. K. Applications of nano-catalyst in new era. *J. Saudi Chem. Soc.* **16**(3), 307–325. <https://doi.org/10.1016/j.jscs.2011.01.015> (2012).
- Baskar, G. & Aiswarya, R. Trends in catalytic production of biodiesel from various feedstocks. *Renew. Sust. Energ. Rev.* **57**, 496–504. <https://doi.org/10.1016/j.rser.2015.12.101> (2016).
- Wang, W., Wang, S., Ma, X. & Gong, J. Recent advances in catalytic hydrogenation of carbon dioxide. *Chem. Soc. Rev.* **40**(7), 3703–3727. <https://doi.org/10.1039/C1CS15008A> (2011).
- Anastas, P. T., Kirchhoff, M. M. & Williamson, T. C. Catalysis as a foundational pillar of green chemistry. *Appl. Catal. A Gen.* **221**(1–2), 3–13. [https://doi.org/10.1016/S0926-860X\(01\)00793-1](https://doi.org/10.1016/S0926-860X(01)00793-1) (2001).
- Council, N. R., Engineering, D. O. & Sciences, P. National Research Council, Division on Engineering and Physical Sciences, Commission on Physical Sciences, Mathematics, and Applications, Panel on New Directions in Catalytic Science and Technology, *Catalysis Looks to the Future*. 0309045843 (National Academies Press, 1992).
- Rehman, A., Noor, T., Hussain, A., Iqbal, N. & Jahan, Z. Role of catalysis in biofuels production process—a review. *ChemBioEng. Rev.* **8**(5), 417–438. <https://doi.org/10.1002/cben.202000040> (2021).
- Gawande, M. B., Zboril, R., Malgras, V. & Yamauchi, Y. Integrated nanocatalysts: A unique class of heterogeneous catalysts. *J. Mater. Chem. A* **3**(16), 8241–8245. <https://doi.org/10.1039/C5TA00119F> (2015).
- Xu, L., Wu, X.-C. & Zhu, J.-J. Green preparation and catalytic application of Pd nanoparticles. *Nanotechnology* **19**(30), 305603. <https://doi.org/10.1088/0957-4484/19/30/305603> (2008).
- Lin, C.-C. et al. Zr-MOF/polyaniline composite films with exceptional seebeck coefficient for thermoelectric material applications. *ACS Appl. Mater. Interfaces* **11**(3), 3400–3406. <https://doi.org/10.1021/acsami.8b17308> (2018).
- Astruc, D., Lu, F. & Aranzas, J. R. Nanoparticles as recyclable catalysts: The Frontier between homogeneous and heterogeneous catalysis. *Angew. Chem. Int. Ed.* **44**(48), 7852–7872. <https://doi.org/10.1002/anie.200500766> (2005).
- Liu, L. & Corma, A. Metal catalysts for heterogeneous catalysis: From single atoms to nanoclusters and nanoparticles. *Chem. Rev.* **118**(10), 4981–5079. <https://doi.org/10.1021/acs.chemrev.7b00776> (2018).

27. Wang, S., Wang, Z. & Zha, Z. Metal nanoparticles or metal oxidenanoparticles, an efficient and promising family of novel heterogeneous catalysts in organic synthesis. *Dalton Trans.* **43**, 9363–9373. <https://doi.org/10.1039/B913539A> (2009).
28. Pan, Y. et al. Size-dependent cytotoxicity of gold nanoparticles. *Small* **3**(11), 1941–1949. <https://doi.org/10.1002/sml.200700378> (2007).
29. Mohammadi, L. et al. Gold nanoparticle decorated post-synthesis modified UiO-66-NH₂ for A³-coupling preparation of propargyl amines. *Sci. Rep.* **13**(1), 9051. <https://doi.org/10.1038/s41598-023-35848-4> (2023).
30. Liu, Y., Wang, J., Li, T., Zhao, Z. & Pang, W. Base-free Pd-MOF catalyzed the Suzuki-Miyaura cross-coupling reaction of arenediazonium tetrafluoroborate salts with arylboronic acids. *Tetrahedron* **75**(40), 130540. <https://doi.org/10.1016/j.tet.2019.130540> (2019).
31. Gole, B., Sanyal, U., Banerjee, R. & Mukherjee, P. S. High loading of Pd nanoparticles by interior functionalization of MOFs for heterogeneous catalysis. *Inorg. Chem.* **55**, 2345–2354. <https://doi.org/10.1021/acs.inorgchem.5b02739> (2016).
32. Xamena, F. X., Abad, A., Corma, A. & Garcia, H. MOFs as catalysts: Activity, reusability and shape-selectivity of a Pd-containing MOF. *J. Catal.* **250**(2), 294–298. <https://doi.org/10.1016/j.jcat.2007.06.004> (2007).
33. Chen, H. & Li, Y. One-pot synthesis of Pd@MOF composites without the addition of stabilizing agents. *Chem. Commun.* **50**(94), 14752–14755. <https://doi.org/10.1039/C4CC06568A> (2014).
34. Mohammadi, L. & Vaezi, M. R. Palladium nanoparticle-decorated porous metal-organic-framework (Zr)@guanidine: Novel efficient catalyst in cross-coupling (Suzuki, Heck, and Sonogashira) reactions and carbonylative Sonogashira under mild conditions. *ACS Omega* **8**(18), 16395–16410. <https://doi.org/10.1021/acsomega.3c01179> (2023).
35. Mohammadi, L., Hosseini, M. & Vaezi, M. R. Stabilization of palladium-nanoparticle-decorated postsynthesis-modified Zr-UiO-66 MOF as a reusable heterogeneous catalyst in C-C coupling reaction. *ACS Omega* **8**(9), 8505–8518. <https://doi.org/10.1021/acsomega.2c07661> (2023).
36. Kitagawa, S. Metal-organic frameworks (MOFs). *Chem. Soc. Rev.* **43**(16), 5415–5418. <https://doi.org/10.1039/C4CS90059F> (2014).
37. Furukawa, H., Cordova, K. E., O'Keeffe, M. & Yaghi, O. M. The chemistry and applications of metal-organic frameworks. *Science* **341**(6149), 1230444. <https://doi.org/10.1126/science.1230444> (2013).
38. James, S. L. Metal-organic frameworks. *Chem. Soc. Rev.* **32**(5), 276–288. <https://doi.org/10.1039/B200393G> (2003).
39. Zhou, H.-C., Long, J. R. & Yaghi, O. M. Introduction to metal-organic frameworks. *Chem. Rev.* **112**, 673–674. <https://doi.org/10.1021/cr300014x> (2012).
40. MacGillivray, L. R. *Metal-Organic Frameworks: Design and Application* (Wiley, 2010).
41. Li, B., Wen, H. M., Cui, Y., Zhou, W. & Chen, B. Emerging multifunctional metal-organic framework materials. *Adv. Mater.* **28**, 8819–8860. <https://doi.org/10.1002/adma.01601133> (2016).
42. Berijani, K. & Morsali, A. The role of metal-organic porous frameworks in dual catalysis. *Inorg. Chem. Front.* **8**(15), 3618–3658. <https://doi.org/10.1039/D1QI00394A> (2021).
43. Huang, X. et al. Research progress of metal organic frameworks and their derivatives for adsorption of anions in water: A review. *Environ. Res.* **204**, 112381 (2022).
44. Daliran, S., Oveisi, A. R., Peng, Y., López-Magano, A. & Khajeh, M. Metal-organic framework (MOF), covalent-organic framework (COF)-, and porous-organic polymers (POP)-catalyzed selective C-H bond activation and functionalization reactions. *Chem. Soc. Rev.* **51**(18), 7810–7882. <https://doi.org/10.1039/D1CS00976A> (2022).
45. Mohmeyer, A. Synthesis, characterization and postsynthetic modification of a novel two-dimensional Zr-based metal-organic framework. <https://doi.org/10.15488/9176> (2019).
46. Ahmadijokani, F. et al. UiO-66 metal-organic frameworks in water treatment: A critical review. *Prog. Mater. Sci.* **125**, 100904. <https://doi.org/10.1016/j.pmatsci.2021.100904> (2022).
47. Dhakshinamoorthy, A., Santiago-Portillo, A., Asiri, A. M. & Garcia, H. Engineering UiO-66 metal organic framework for heterogeneous catalysis. *ChemCatChem* **11**(3), 899–923. <https://doi.org/10.1002/cctc.201801452> (2019).
48. Yang, L.-M., Ganz, E., Svelle, S. & Tilset, M. Computational exploration of newly synthesized zirconium metal-organic frameworks UiO-66, -67, -68 and analogues. *J. Mater. Chem. C* **2**(34), 7111–7125. <https://doi.org/10.1039/C4TC00902A> (2014).
49. Vahabi, A. H., Norouzi, F., Sheibani, E. & Rahimi-Nasrabadi, M. Functionalized Zr-UiO-67 metal-organic frameworks: Structural landscape and application. *Coord. Chem. Rev.* **445**, 214050. <https://doi.org/10.1016/j.ccr.2021.214050> (2021).
50. Xu, R., Kang, Y., Zhang, W., Zhang, X. & Pan, B. Oriented UiO-67 metal-organic framework membrane with fast and selective lithium-ion transport. *Angew. Chem. Int. Ed.* **61**(3), e202115443. <https://doi.org/10.1002/anie.202115443> (2022).
51. Ye, X. & Liu, D. Metal-organic framework UiO-68 and its derivatives with sufficiently good properties and performance show promising prospects in potential industrial applications. *Cryst. Growth Des.* **21**(8), 4780–4804. <https://doi.org/10.1021/acs.cgd.1c00460> (2021).
52. Li, M., Yuan, D., Wu, B. & Hong, M. Engineering UiO-68-typed homochiral metal-organic frameworks for the enantiomeric separation of Fmoc-AAAs and mechanism study. *ACS Appl. Mater. Interfaces* **15**(18), 22241–22250. <https://doi.org/10.1021/acsam.1c01735> (2023).
53. Li, M., Zhang, L., Wu, B. & Hong, M. High-enantioselectivity adsorption separation of racemic mandelic acid and methyl mandelate by robust chiral UiO-68-Type Zr-MOFs. *Inorg. Chem.* **63**(1), 381–389. <https://doi.org/10.1021/acs.inorgchem.3c03277> (2023).
54. Lawrence, M. C. & Katz, M. J. Analysis of the water adsorption isotherms in UiO-based metal-organic frameworks. *J. Phys. Chem. C* **126**(2), 1107–1114. <https://doi.org/10.1021/acs.jpcc.1c05190> (2021).
55. Zou, D. & Liu, D. Understanding the modifications and applications of highly stable porous frameworks via UiO-66. *Mater. Today Chem.* **12**, 139–165. <https://doi.org/10.1016/j.mtchem.2018.12.004> (2019).
56. Winarta, J. et al. A decade of UiO-66 research: A historic review of dynamic structure, synthesis mechanisms, and characterization techniques of an archetypal metal-organic framework. *Cryst. Growth Des.* **20**(2), 1347–1362. <https://doi.org/10.1021/acs.cgd.9b00955> (2019).
57. Katz, M., Brown, Z., Colón, Y. & Siu, P. K. A facile synthesis of UiO-66, UiO-67 and their derivatives. *Chem. Commun.* **49**, 9449–9451. <https://doi.org/10.1039/C3CC46105J> (2013).
58. Kandiah, M. et al. Synthesis and stability of tagged UiO-66 Zr-MOFs. *Chem. Mater.* **22**(24), 6632–6640. <https://doi.org/10.1021/cm102601v> (2010).
59. Trickett, C. A. et al. Definitive molecular level characterization of defects in UiO-66 crystals. *Angew. Chem. Int. Ed.* **54**(38), 11162–11167. <https://doi.org/10.1002/anie.201505461> (2015).
60. Li, Y.-H., Wang, C.-C., Yi, X.-H. & Chu, H.-Y. UiO-66(Zr)-based functional materials for water purification: An updated review. *Environ. Funct. Mater.* **2**, 93–132. <https://doi.org/10.1016/j.efmat.2024.02.001> (2023).
61. Luu, C. L., Van Nguyen, T. T., Nguyen, T. & Hoang, T. C. Synthesis, characterization and adsorption ability of UiO-66-NH₂. *Adv. Sci. Nanosci. Nanotechnol.* **6**(2), 025004. <https://doi.org/10.1088/2043-6262/6/2/025004> (2015).
62. Hajek, J. et al. Mechanistic studies of aldol condensations in UiO-66 and UiO-66-NH₂ metal organic frameworks. *J. Catal.* **331**, 1–12. <https://doi.org/10.1016/j.jcat.2015.08.015> (2015).
63. Vermoortele, F. et al. Synthesis modulation as a tool to increase the catalytic activity of metal-organic frameworks: The unique case of UiO-66(Zr). *J. Am. Chem. Soc.* **135**(31), 11465–11468. <https://doi.org/10.1021/ja405078u> (2013).

64. Hua, W., Zhang, T., Wang, M., Zhu, Y. & Wang, X. Hierarchically structural PAN/UiO-66-(COOH)₂ nanofibrous membranes for effective recovery of Terbium(III) and Europium(III) ions and their photoluminescence performances. *Chem. Eng. J.* **370**, 729–741. <https://doi.org/10.1016/j.cej.2019.03.255> (2019).
65. Wang, K., Wu, J., Zhu, M., Zheng, Y.-Z. & Tao, X. Highly effective pH-universal removal of tetracycline hydrochloride antibiotics by UiO-66-(COOH)₂/GO metal-organic framework composites. *J. Solid State Chem.* **284**, 121200. <https://doi.org/10.1016/j.jssc.2020.121200> (2020).
66. Feng, L., Liu, J., Abu-Hamdeh, N. H., Bezzina, S. & Malekshah, R. E. Molecular dynamics and quantum simulation of different cationic dyes removal from contaminated water using UiO-66 (Zr)-(COOH)₂ metal-organic framework. *J. Mol. Liq.* **349**, 118085. <https://doi.org/10.1016/j.molliq.2021.118085> (2022).
67. Dinh, H. T., Tran, N. T. & Trinh, D. X. Investigation into the adsorption of methylene blue and methyl orange by UiO-66-NO₂ nanoparticles. *J. Anal. Methods Chem.* **1**, 5512174. [https://doi.org/10.1155/2021/5512174\(2021\)](https://doi.org/10.1155/2021/5512174(2021)) (2021).
68. Zeng, S. et al. UiO-66-NO₂ as an oxygen “Pump” for enhancing oxygen reduction reaction performance. *Chem. Mater.* **31**(5), 1646–1654. <https://doi.org/10.1021/acs.chemmater.8b04934> (2019).
69. Rada, Z., Abid, H. R., Sun, H. & Wang, S. Bifunctionalized metal organic frameworks, UiO-66-NO₂-N (N = -NH₂, -(OH)₂, (COOH)₂), for enhanced adsorption and selectivity of CO₂ and N₂. *J. Chem. Eng. Data* **60**(7), 2152–2161. <https://doi.org/10.1021/acs.jced.5b00229> (2015).
70. Wang, C. et al. Amorphous metal-organic framework UiO-66-NO₂ for removal of oxyanion pollutants: Towards improved performance and effective reusability. *Sep. Purif. Technol.* **295**, 121014. <https://doi.org/10.1016/j.seppur.2022.121014> (2022).
71. Bahar, M. K., Khan, W. U., Helal, A. & Al-Harthi, M. A. Inscriptions of metal organic frame work (MOF) reinforcements in polymeric nanocomposites—state-of-the-art and multifaceted impressions. *Polym. Plast. Technol. Mater.* **63**(1), 38–54. <https://doi.org/10.1080/25740881.2024.2441941> (2024).
72. Schelling, M., Otal, E., Kim, M. & Hinestroza, J. P. Conformal functionalization of cotton fibers via isoreticular expansion of UiO-66 metal-organic frameworks. *Coatings* **10**(12), 1172. <https://doi.org/10.3390/coatings10121172> (2020).
73. Jia, X. et al. Highly efficient photocatalytic degradation of tetracycline by modifying UiO-66 via different regulation strategies. *ACS Omega* **8**(30), 27375–27385. <https://doi.org/10.1021/acsomega.3c02762> (2023).
74. Verma, R. et al. Amine-decorated zirconium based metal organic framework for ultrafast detection of 2,4,6-trinitrophenol in aqueous samples. *J. Fluoresc.* **33**(5), 2085–2098. <https://doi.org/10.1007/s10895-023-03216-0> (2023).
75. Kung, C.-W. et al. Charge transport in Zirconium-based metal-organic frameworks. *Acc. Chem. Res.* **53**(6), 1187–1195. <https://doi.org/10.1021/acs.accounts.0c00106> (2020).
76. Gómez-Avilés, A., Solís, R. R., García-Frutos, E. M., Bedia, J. & Belver, C. Novel isoreticular UiO-66-NH₂ frameworks by N-cycloalkyl functionalization of the 2-aminoterephthalate linker with enhanced solar photocatalytic degradation of acetaminophen. *Chem. Eng. J.* **461**, 141889. <https://doi.org/10.1016/j.cej.2023.141889> (2023).
77. Bunge, M. A., Davis, A. B., West, K. N., West, C. W. & Glover, T. G. Synthesis and characterization of UiO-66-NH₂ metal-organic framework cotton composite textiles. *Ind. Eng. Chem. Res.* **57**(28), 9151–9161. <https://doi.org/10.1021/acs.iecr.8b01010> (2018).
78. Szejtli, J. Introduction and general overview of cyclodextrin chemistry. *Chem. Rev.* **98**(5), 1743–1754 (1998).
79. Davis, M. E. & Brewster, M. E. Cyclodextrin-based pharmaceuticals: Past, present and future. *Nat. Rev. Drug Dis.* **3**(12), 1023–1035. <https://doi.org/10.1038/nrd1576> (2004).
80. Bender, M. L. & Komiyama, M. *Cyclodextrin Chemistry* Vol. 6 (Springer Science & Business Media, 2012). <https://doi.org/10.1007/978-3-642-66842-5>.
81. Szejtli, J. Past, present and future of cyclodextrin research. *Pure Appl. Chem.* **76**(10), 1825–1845 (2004).
82. Szejtli, J. *Cyclodextrin Technology* Vol. 1 (Springer Science & Business Media, 1988).
83. Poulson, B. G. et al. Cyclodextrins: Structural, chemical, and physical properties, and applications. *Polysaccharides* **3**(1), 1–31. <https://doi.org/10.3390/polysaccharides3010001> (2022).
84. Kurkov, S. V. & Loftsson, T. Cyclodextrins. *Int. J. Pharm.* **453**(1), 167–180. <https://doi.org/10.1016/j.ijpharm.2012.06.055> (2013).
85. Stella, V. J. & He, Q. Cyclodextrins. *Toxicol. Pathol.* **36**(1), 30–42. <https://doi.org/10.1177/0192623307310945> (2008).
86. Crini, G. Review: A history of cyclodextrins. *Chem. Rev.* **114**(21), 10940–10975. <https://doi.org/10.1021/cr500081p> (2014).
87. Del Valle, M. E. Cyclodextrins and their uses: A review. *Process Biochem.* **39**(9), 1033–1046. [https://doi.org/10.1016/S0032-9592\(03\)00258-9](https://doi.org/10.1016/S0032-9592(03)00258-9) (2004).
88. Gonzalez Pereira, A. et al. Main applications of cyclodextrins in the food industry as the compounds of choice to form host–guest complexes. *Int. J. Mol. Sci.* **22**(3), 1339. <https://doi.org/10.3390/ijms22031339> (2021).
89. Fernández, M. A., Silva, O. F., Vico, R. V. & de Rossi, R. H. Complex systems that incorporate cyclodextrins to get materials for some specific applications. *Carbohydr. Res.* **480**, 12–34. <https://doi.org/10.1016/j.carres.2019.05.006> (2019).
90. Wüpper, S., Lüersen, K., Lüersen, G. & Cyclodextrins, G. Natural compounds, and plant bioactives—a nutritional perspective. *Biomolecules* **11**(3), 401. <https://doi.org/10.3390/biom11030401> (2021).
91. Lee, D. T., Zhao, J. C., Oldham, J., Peterson, G. W. & Parsons, G. N. UiO-66-NH₂ metal-organic framework (MOF) nucleation on TiO₂, ZnO, and Al₂O₃ atomic layer deposition-treated polymer fibers: Role of metal oxide on MOF growth and catalytic hydrolysis of chemical warfare agent simulants. *ACS Appl. Mater. Interfaces* **9**(51), 44847–44855. <https://doi.org/10.1021/acsami.7b15397> (2017).
92. Zhang, H., Liu, Z. & Shen, J. Cyclodextrins modified/coated metal-organic frameworks. *Materials* **13**(6), 1273. <https://doi.org/10.3390/ma13061273> (2020).
93. Maesta Bezerra, F. et al. The role of β-cyclodextrin in the textile industry—review. *Molecules* **25**(16), 3624–3628. <https://doi.org/10.3390/molecules25163624> (2020).
94. Decock, G., Landy, D., Surpateanu, G. & Fourmentin, S. Study of the retention of aroma components by cyclodextrins by static headspace gas chromatography. *J. Incl. Phenom. Macrocycl. Chem.* **62**(3), 297–302. <https://doi.org/10.1007/s10847-008-9471-z> (2008).
95. Pratt, D. Y., Wilson, L. D., Kozinski, J. A. & Mohart, A. M. Preparation and sorption studies of β-cyclodextrin/epichlorohydrin copolymers. *J. Appl. Polym. Sci.* **116**(5), 2982–2989. <https://doi.org/10.1002/app.31824> (2010).
96. Hamed, A., Anceschi, A., Patrucco, A. & Hasanzadeh, M. A γ-cyclodextrin-based metal-organic framework (γ-CD-MOF): A review of recent advances for drug delivery application. *J. Drug Target.* **30**(4), 381–393. <https://doi.org/10.1080/1061186X.2021.2012683> (2022).
97. He, S. et al. Metal-organic frameworks for advanced drug delivery. *Acta Pharm. Sin. B.* **11**(8), 2362–2395. <https://doi.org/10.1016/j.apsb.2021.03.019> (2021).
98. Rao, C. R., Kulkarni, G. U., Thomas, P. J. & Edwards, P. P. Metal nanoparticles and their assemblies. *Chem. Soc. Rev.* **29**, 27–35. <https://doi.org/10.1039/A904518J> (2000).
99. Blessy Rebecca, P. N., Durgalakshmi, D. & Ajay Rakesh, R. Metal-organic frameworks (MOFs) for glucose sensing: Advancing non-invasive detection strategies in diabetes management. *Anal. Sens.* **5**(1), e202300052. <https://doi.org/10.1002/anse.202400078> (2025).
100. Basak, S. et al. Metal-organic framework as nanocarriers for agricultural applications: A review. *Front. Nanotechnol.* **6**, 1385981. <https://doi.org/10.3389/fnano.2024.1385981> (2024).

101. Hoyez, G., Rousseau, J., Rousseau, C., Saitzek, S., King, J., Szilágyi, P. Á., Volklinger, C., Loiseau, T., Hapiot, F. & Monflier, E. Cyclodextrins: A new and effective class of co-modulators for aqueous zirconium-MOF syntheses *CrystEngComm*. **23**(14), 2764–2772. <https://doi.org/10.1039/D1CE00128K> (2021).
102. Liu, F. & Hu, B. Experimental and DFT study of adsorption-reduction mechanism of Au(III) and Cr(VI) by β -cyclodextrin/polydopamine coated UiO-66-NH₂ magnetic composites. *Appl. Surf. Sci.* **626**, 157292. <https://doi.org/10.1016/j.apsusc.2023.157292> (2023).
103. Lin, S., Gan, N., Cao, Y., Chen, Y. & Jiang, Q. Selective dispersive solid phase extraction-chromatography tandem mass spectrometry based on aptamer-functionalized UiO-66-NH₂ for determination of polychlorinated biphenyls. *J. Chromatogr. A*. **1446**, 34–40. <https://doi.org/10.1016/j.chroma.2016.04.016> (2016).
104. Mohammadi, L. et al. Stabilization of Pd NPs over the surface of β -cyclodextrin incorporated UiO-66-NH₂ for the C-C coupling reaction. *RSC Adv.* **13**(25), 17143–17154. <https://doi.org/10.1039/D2RA08347G> (2023).
105. Yao, X., Huang, P. & Nie, Z. Cyclodextrin-based polymer materials: From controlled synthesis to applications. *Prog. Polym. Sci.* **93**, 1–35. <https://doi.org/10.1016/j.progpolymsci.2019.03.004> (2019).
106. Van De Manacker, F., Vermonden, T., Van Nostrum, C. F. & Hennink, W. E. Cyclodextrin-based polymeric materials: Synthesis, properties, and pharmaceutical/biomedical applications. *Biomacromol* **10**(12), 3157–3175. <https://doi.org/10.1021/bm901065f> (2009).
107. Okasha, A. T. et al. Progress of synthetic cyclodextrins-based materials as effective adsorbents of the common water pollutants: Comprehensive review. *J. Environ. Chem. Eng.* **11**(3), 109824. <https://doi.org/10.1016/j.jece.2023.109824> (2023).
108. Concheiro, A. & Alvarez-Lorenzo, C. Chemically cross-linked and grafted cyclodextrin hydrogels: From nanostructures to drug-eluting medical devices. *Adv. Drug Deliv. Rev.* **65**(9), 1188–1203. <https://doi.org/10.1016/j.addr.2013.04.015> (2013).
109. Li, Y., Hong, X. M., Collard, D. M. & El-Sayed, M. A. Suzuki cross-coupling reactions catalyzed by palladium nanoparticles in aqueous solution. *Org. Lett.* **2**, 2385–2388. <https://doi.org/10.1021/ol0061687> (2000).
110. Zhang, Y., Huang, J. & Ding, Y. Porous Co₃O₄/CuO hollow polyhedral nanocages derived from metal-organic frameworks with heterojunctions as efficient photocatalytic water oxidation catalysts. *Appl. Catal. B Environ.* **198**, 447–456. <https://doi.org/10.1016/j.apcatb.2016.05.078> (2016).
111. Fedlheim, D. L. & Foss, C. A. *Metal Nanoparticles: Synthesis, Characterization, and Applications* (CRC Press, 2001).
112. Babu, P. J. & Tirkey, A. Green synthesis of gold nanoparticles and their biomedical and healthcare applications. *Nanotechnol. Hum. Health* <https://doi.org/10.1016/B978-0-323-90750-7.00006-5> (2023).
113. Cuenya, B. R. Synthesis and catalytic properties of metal nanoparticles: Size, shape, support, composition, and oxidation state effects. *Thin Solid Films* **518**(12), 3127–3150. <https://doi.org/10.1016/j.tsf.2010.01.018> (2010).
114. Narayan, N., Meiyazhagan, A. & Vajtai, R. Metal nanoparticles as green catalysts. *Materials* **12**(21), 3602. <https://doi.org/10.3390/ma12213602> (2019).
115. Reina, A., Dang-Bao, T., Guerrero-Ríos, I. & Gómez, M. Palladium and copper: Advantageous nanocatalysts for multi-step transformations. *Nanomaterials* **11**(8), 1891. <https://doi.org/10.3390/nano11081891> (2021).
116. de Barros, S. D., Senra, J. D., Lachter, E. R. & Malta, L. F. Metal-catalyzed cross-coupling reactions with supported nanoparticles: Recent developments and future directions. *Catal. Rev.* **58**, 439–496. <https://doi.org/10.1080/01614940.2016.1202640> (2016).
117. Mohammadi, L. et al. Stabilization of copper nanoparticles onto the double Schiff-base-functionalized ZSM-5 for A³ coupling reaction catalysis aimed under mild conditions. *RSC Adv.* **13**(7), 4843–4858. <https://doi.org/10.1039/D2RA07700K> (2023).
118. Abánades Lázaro, L., Wells, C. J. & Forgan, R. S. Multivariate modulation of the Zr MOF UiO-66 for defect-controlled combination anticancer drug delivery. *Angew. Chem.* **132**(13), 5249–5255. <https://doi.org/10.1002/ange.201915848> (2020).
119. Ferahia, A., Halilat, M. T., Mimeche, F. & Bensaci, E. Surface water quality assessment in semi-arid region (El Hodna watershed, Algeria) based on water quality index (WQI). *Stud. Univ. Babeş-Bolyai, Chem.* **66**(1), 127–142. <https://doi.org/10.24193/subbchem.2021.1.10> (2021).
120. Krishnamurthy, S., Esterle, A., Sharma, N. C. & Sahi, S. V. Yucca-derived synthesis of gold nanomaterial and their catalytic potential. *Nanoscale Res. Lett.* **9**, 1–9. <https://doi.org/10.1186/1556-276X-9-627> (2014).
121. Sun, J., Fu, Y., He, G., Sun, X. & Wang, X. Green Suzuki-Miyaura coupling reaction catalyzed by palladium nanoparticles supported on graphitic carbon nitride. *Appl. Catal. B Environ.* **165**, 661–667. <https://doi.org/10.1016/j.apcatb.2014.10.072> (2015).
122. Raheem, A. A., Thangasamy, P., Sathish, M. & Praveen, C. Supercritical water assisted preparation of recyclable gold nanoparticles and their catalytic utility in cross-coupling reactions under sustainable conditions. *Nanoscale Adv.* **1**(8), 3177–3191. <https://doi.org/10.1039/C9NA00240E> (2019).
123. Shaw, B. L. Highly active, stable, catalysts for the Heck reaction; further suggestions on the mechanism. *Chem. Commun.* **13**, 1361–1362. <https://doi.org/10.1039/A802642D> (1998).
124. Liao, Y. et al. Magnetite nanoparticle-supported coordination polymer nanofibers: Synthesis and catalytic application in Suzuki-Miyaura coupling. *ACS Appl. Mater. Interfaces*. **2**(8), 2333–2338. <https://doi.org/10.1021/am100354b> (2010).
125. Borhade, S. R. & Waghmode, S. B. Studies on Pd/NiFe₂O₄ catalyzed ligand-free Suzuki reaction in aqueous phase: Synthesis of biaryls, terphenyls and polyaryls. *Beilstein J. Org. Chem.* **7**(1), 310–319 (2011).
126. Elazab, H. A., Siamaki, A. R., Moussa, S., Gupton, B. F. & El-Shall, M. S. Highly efficient and magnetically recyclable graphene-supported Pd/Fe₃O₄ nanoparticle catalysts for Suzuki and Heck cross-coupling reactions. *Appl. Catal. A Gen.* **491**, 58–69. <https://doi.org/10.1016/j.apcata.2014.11.033> (2015).
127. Zeltner, M., Schätz, A. & Hefti, M. L. Magnetothermally responsive C/Co@PNIPAM-nanoparticles enable preparation of self-separating phase-switching palladiumcatalysts. *J. Mater. Chem.* **21**(9), 2991–2996. <https://doi.org/10.1039/C0JM03338C> (2011).
128. Faisal, S. *ROMP-Derived Alkylating Reagents and Scavengers: Application in Library Development and Sequestration* (University of Kansas, 2016).
129. Li, R. et al. Pd-Fe₃O₄/C hybrid nanoparticles: Preparation, characterization, and their high catalytic activity toward Suzuki coupling reactions. *J. Mater. Chem.* **22**(42), 22750–22755. <https://doi.org/10.1039/C2JM35252D> (2012).
130. Amali, A. J. & Rana, R. K. Stabilization of Pd(0) on surface functionalised Fe₃O₄ nanoparticles: Magnetically recoverable and stable recyclable catalyst for hydrogenation and Suzuki-Miyaura reactions. *Green Chem.* **11**(11), 1781–1786. <https://doi.org/10.1039/B916261P> (2009).
131. Yang, J. et al. Palladium supported on a magnetic microgel: An efficient and recyclable catalyst for Suzuki and Heck reactions in water. *Green Chem.* **15**(12), 3429–3437. <https://doi.org/10.1039/C3GC40941D> (2013).
132. Tanhaei, M., Mahjoub, A. & Nejat, R. Three-dimensional graphene-magnetic palladium nanohybrid: A highly efficient and reusable catalyst for promoting organic reactions. *Catal. Lett.* **148**(6), 1549–1561. <https://doi.org/10.1007/s10562-018-2347-y> (2018).
133. Kwon, T. H., Cho, K. Y., Baek, K.-Y., Yoon, H. G. & Kim, B. M. Recyclable palladium-graphene nanocomposite catalysts containing ionic polymers: Efficient Suzuki coupling reactions. *RSC Adv.* **7**(19), 11684–11690. <https://doi.org/10.1039/C6RA26998B> (2017).
134. Park, J. H. et al. Recyclable N-heterocyclic carbene/palladium catalyst on graphene oxide for the aqueous-phase Suzuki reaction. *Tetrahedron Lett.* **55**(23), 3426–3430. <https://doi.org/10.1016/j.tetlet.2014.04.078> (2014).
135. Wang, Z. J., Ghasimi, S., Landfester, K. & Zhang, K. A. Photocatalytic Suzuki coupling reaction using conjugated microporous polymer with immobilized palladium nanoparticles under visible light. *Chem. Mater.* **27**(6), 1921–1924. <https://doi.org/10.1021/acs.chemmater.5b00516> (2015).

136. Dong, D. et al. Postsynthetic modification of single Pd sites into uncoordinated polypyridine groups of a MOF as the highly efficient catalyst for Heck and Suzuki reactions. *New J. Chem.* **42**(11), 9317–9323. <https://doi.org/10.1039/C8NJ00518D> (2018).
137. Singh, R. et al. Solid-supported materials-based synthesis of 2-substituted benzothiazoles: Recent developments and Sanguine future. *ChemistrySelect* **6**(25), 6388–6449. <https://doi.org/10.1002/slct.202101368> (2021).
138. Bahrami, K. & Kamrani, S. N. Synthesis, characterization and application of graphene palladium porphyrin as a nanocatalyst for the coupling reactions such as: Suzuki-Miyaura and Mizoroki-Heck. *Appl. Organomet. Chem.* **32**(2), e4102. <https://doi.org/10.1002/aoc.4102> (2018).

Acknowledgements

The authors would like to thank the Materials and Energy Research Center (Grant No.: 9911940) and especially grateful of Iran's National Elites Foundation (INEF) for the financial support of this project

Author contributions

Leila Mohammadi was responsible for synthesizing the UiO-66-NH₂@Epichlorohydrin/CD/Au-NPs catalyst, conducting the C-C coupling and Carbonylative Sonogashira reactions, and preparing and assembling the manuscript. Mohammad Reza Vaezi provided valuable contributions to the manuscript's editing.

Declarations

Competing interests

The authors declare no competing interests.

Additional information

Supplementary Information The online version contains supplementary material available at <https://doi.org/10.1038/s41598-025-97624-w>.

Correspondence and requests for materials should be addressed to L.M. or M.V.

Reprints and permissions information is available at www.nature.com/reprints.

Publisher's note Springer Nature remains neutral with regard to jurisdictional claims in published maps and institutional affiliations.

Open Access This article is licensed under a Creative Commons Attribution-NonCommercial-NoDerivatives 4.0 International License, which permits any non-commercial use, sharing, distribution and reproduction in any medium or format, as long as you give appropriate credit to the original author(s) and the source, provide a link to the Creative Commons licence, and indicate if you modified the licensed material. You do not have permission under this licence to share adapted material derived from this article or parts of it. The images or other third party material in this article are included in the article's Creative Commons licence, unless indicated otherwise in a credit line to the material. If material is not included in the article's Creative Commons licence and your intended use is not permitted by statutory regulation or exceeds the permitted use, you will need to obtain permission directly from the copyright holder. To view a copy of this licence, visit <http://creativecommons.org/licenses/by-nc-nd/4.0/>.

© The Author(s) 2025